Z-source Circuit Breakers in Naval Power Systems

by

William T. Taft

B.S., United States Naval Academy (2005)
M.E.M., Old Dominion University (2017)

Submitted to the Department of Mechanical Engineering and
Department of Electrical Engineering and Computer Science
in partial fulfillment of the requirements for the degrees of

Naval Engineer

and

Master of Science in Electrical Engineering and Computer Science

at the

MASSACHUSETTS INSTITUTE OF TECHNOLOGY

June 2019

Author ..... Signature redacted .....
Department of Mechanical Engineering and
Department of Electrical Engineering and Computer Science
May 9, 2019

Certified by ..... Signature redacted .....
James L. Kirtley
Professor of Electrical Engineering and Computer Science
Thesis Supervisor

Certified by ..... Signature redacted .....
Steven B. Leeb
Professor of Electrical Engineering and Computer Science
and Mechanical Engineering
Thesis Reader

Accepted by ..... Signature redacted .....
Leslie A. Kolodziejski
Professor of Electrical Engineering and Computer Science
Chair, Department Committee on Graduate Students

Accepted by ..... Signature redacted .....
Nicolas Hadjiconstantinou
Professor of Mechanical Engineering
Chairman, Committee on Graduate Students

Z-source Circuit Breakers in Naval Power Systems

by

William T. Taft

Submitted to the Department of Mechanical Engineering and
Department of Electrical Engineering and Computer Science
on May 9, 2019, in partial fulfillment of the
requirements for the degrees of
Naval Engineer
and
Master of Science in Electrical Engineering and Computer Science

Abstract

New power system components and control systems are required to facilitate the U.S. Navy's move to medium voltage direct current power (MVDC) systems on future vessels. Integrating the z-source circuit breaker into a "typical" naval MVDC power system requires understanding system dynamics that may cause the circuit breaker to inadvertently energize a circuit through regenerative turn-on of the thyristor. An electrically-scaled model and a simulation model are used to characterize voltage transients that could lead to this false triggering. The results of this experiment show that these transients are within the specifications of commercially available components. Limitations in the circuit breaker's protective capabilities during turn-on transients are identified and discussed. Potential topology modifications, control schemes, and power system arrangements that provide protection across the operating range are proposed for further investigation.

Thesis Supervisor: James L. Kirtley
Title: Professor of Electrical Engineering and Computer Science

Acknowledgments

The completion of this thesis and my success at MIT were possible because of the support and encouragement that I received from those around me.

First and foremost I want to thank my wonderful wife Heather for her unwavering support. Three years ago she agreed to move our family to a new city and since then she has managed the daily and long-term operation of our home. She has ensured that I was always able to spend extra time at school or working on problem sets when I needed to do so. As an academic she provided even more support as a sounding board for how to approach part of a paper, giving a quick answer on how to properly cite sources, and invaluable feedback proofreading every important assignment I have submitted.

I would also like to thank Professor James Kirtley. Not only did he welcome me into his lab and provide a supportive environment in which I could complete the work contained within this thesis, he also stimulated my initial interest in power systems as a field of study. Without his guidance and advice I would not have been able to complete this endeavor. Similarly, the other graduate students in his lab helped me through my electrical engineering classes and my experiments, and made sure I knew how to find the resources I needed when I got bogged down.

Finally, I wish to thank the U.S. Navy and the Engineering Duty Officer community for the incredible opportunity they have provided me by funding my graduate education and allowing me the time to pursue my naval engineering studies. I wish to specifically thank CAPT Joe Harbour, CDR Andrew Gillespy, and CDR Jon Page for their support through running the Naval Construction and Engineering program at MIT. I also want to thank my shipmates that have progressed through the program with me for all their support and encouragement along the way.

THIS PAGE INTENTIONALLY LEFT BLANK

Contents

THIS PAGE INTENTIONALLY LEFT BLANK

List of Figures

THIS PAGE INTENTIONALLY LEFT BLANK

List of Tables

THIS PAGE INTENTIONALLY LEFT BLANK

Chapter 1

Background

1.1 Electrification of Ships

Electrification of ships first appeared in the 1870s, starting with small, non-propulsion loads [1]. Initially, individual components were electrified, such as call bells and stand-alone spot lights. The trend toward increasing electrification continued with the installation of the first shipboard electrical distribution system on SS *Columbia* in 1880, used to light the vessel [1]. The U.S. Navy soon followed suit with the installation of an electric lighting system on USS *Trenton* in 1883 [2]. The continued electrification over the past 140 years has grown well beyond lighting, now covering nearly all hotel service loads[1], communications and network devices, fresh water production, and sensors. At this point there is an electrically-powered option for nearly any imaginable task performed on a vessel.

Shipboard electrification was not contained to just the smaller auxiliary and hotel service loads for long, with engineers electrifying propulsion in the early twentieth century. The first large surface vessel with electric propulsion was *Vandal*[2], a Russian river tanker launched in 1903 [1]. *Vandal* used a diesel-electric system similar to that

[1] Hotel service loads are loads such as climate control, hot water production, food preparation, laundry, etc.

[2] *Vandal* is widely recognized as the first electrically propelled ship. Smaller launch-sized boats using battery-powered motors were briefly experimented with in the 1830s, but were found infeasible with motor technology of the time [1]. Additionally, the experimental submarine *Holland*, launched in 1900, used a form of diesel-electric propulsion [3].

used in diesel-electric locomotives. In 1913, the U.S. Navy commissioned the collier USS *Jupiter* (AC 3)[3], its first vessel equipped with an electric propulsion system [4]. Unlike *Vandal*, USS *Jupiter* employed a turbo-electric system with a steam turbine as the prime mover. The U.S. Navy, among others, continued to build large surface vessels that employed turbo-electric propulsion through the 1940s. Most ocean-going icebreakers built since the 1940s have also employed some form of electric propulsion, but it fell out of common use elsewhere.

The next step in the evolution of shipboard electrification was the combination of these two trends into the Integrated Power System (IPS) concept. This began as electric propulsion saw a resurgence in the mid-1980s with the re-engining of the passenger liner *Queen Elizabeth 2* [5], the first large electric[4] IPS vessel [1]. The trend of IPS implementation by naval architects and marine engineers has continued with its use in cruise ships and naval vessels. The U.S. Navy has recently commissioned vessels of a couple different classes employing IPS, including the *Zumwalt*-class guided missile destroyer [7] and the *Lewis and Clark*-class dry cargo/ammunition ships [8].

All of this history, at least for U.S. Navy vessels, is neatly summarized in figure 1-1 [9], which shows that the fraction of the ship used for electrical generation has risen steadily. Similarly, figure 1-2 shows how the U.S. Navy plans to continue this trend in the future.

[3]In 1920 *Jupiter* was renamed *Langley* (CV 1), and converted into the first U.S. Navy aircraft carrier [4].

[4]An *integrated* power system is a shipboard power system in which one form of energy is used to power most or all of the vessel's systems. On naval vessels, IPS can take the form of a steam-based system or an electricity-based system [6]. From here on out, IPS will refer to electricity-based systems unless specifically noted

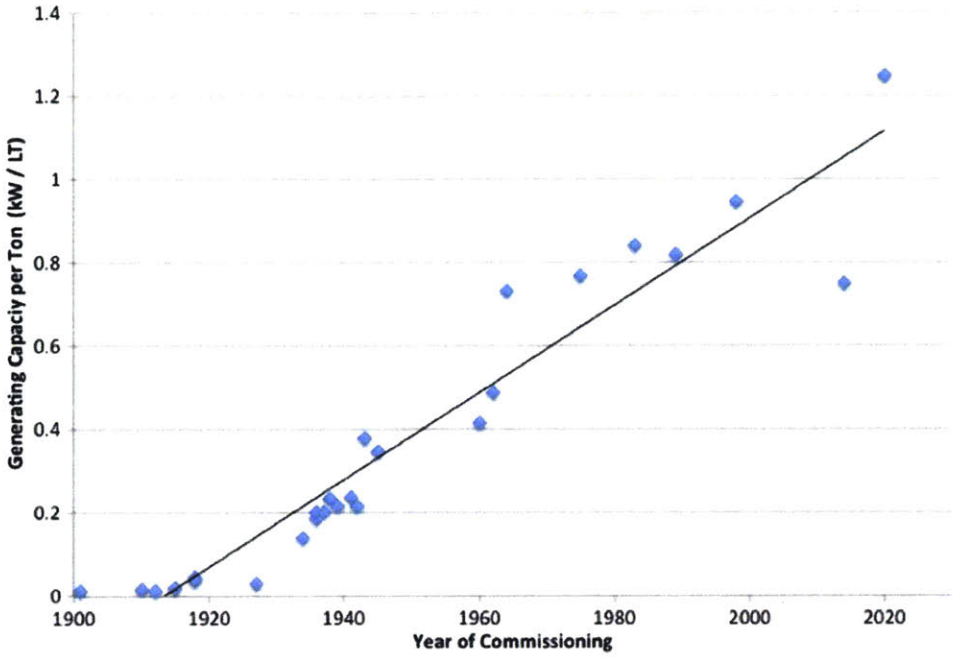

Figure 1-1. Historical U.S. Navy installed electric generating capacity. Source: "Integrated power systems - An outline of requirements and functionalities for ships" [9].

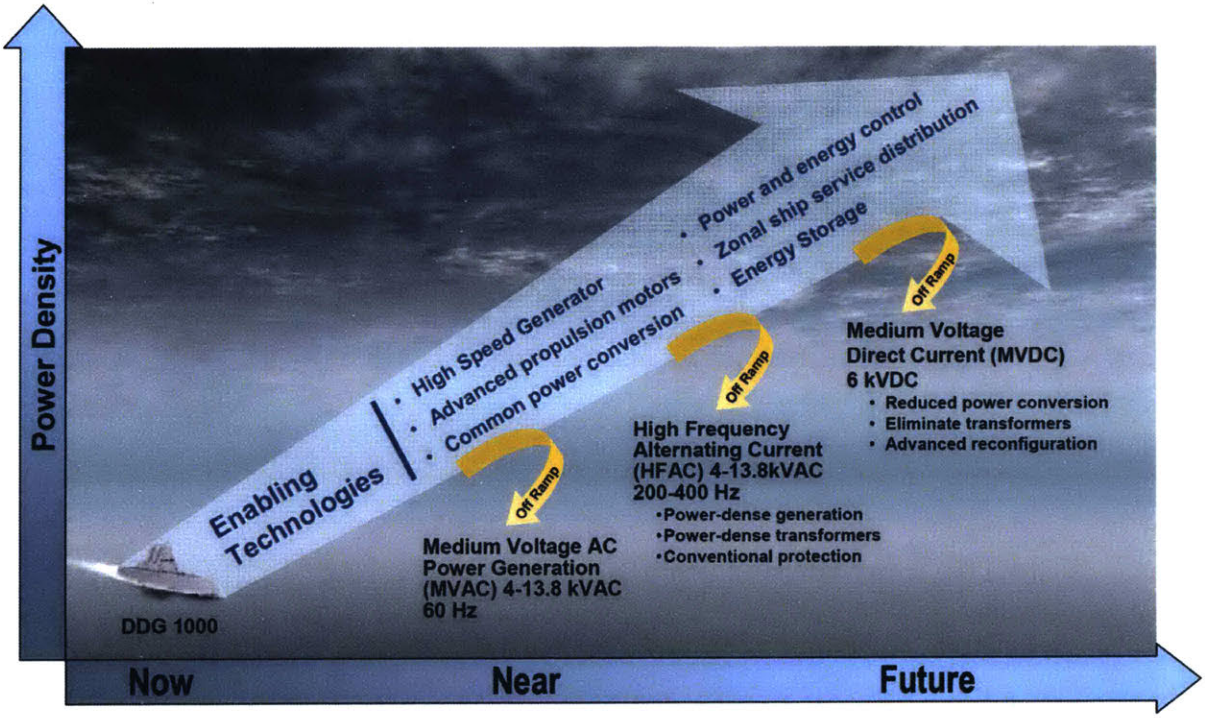

Figure 1-2. Next Generation Integrated Power System Technology Development Roadmap. Source: NAVSEA *NGIPS Technology Development Roadmap* [10].

1.2 Current State of Technology

Most current U.S. Navy ships employ AC electrical distribution systems. These systems operate primarily at 60 Hz. There are some special systems that operate at 400 Hz, such as combat systems and aircraft support, and others that can operate at variable frequencies [11]. Only the *Virginia*-class fast attack submarines use a DC distribution system. Components for systems operating at 60 Hz are readily available and well understood because it is the terrestrial standard in a large part of the world, including the United States. The basic configuration of shipboard systems has remained largely unchanged since the 1940s, when Rickover wrote about the U.S. Navy's scheme for providing fault protection using selective tripping of circuit breakers [12].

As discussed in [10] and illustrated in Figure 1-2, the U.S. Navy desires to move away from 60 Hz AC electrical systems and toward DC electrical systems. The bridging technology is high frequency AC (HFAC). The Naval Sea Systems command (NAVSEA) selected HFAC because it provides some of the advantages of DC systems (e.g., smaller transformers and reduced acoustic signatures) while avoiding some of the developmental investments required by DC systems [10]. DC systems are the ultimate goal, though, because they provide a number of advantages for naval vessels:

- Prime mover speed is decoupled from the system frequency and generators are not limited to specific numbers of poles.
- Power conversion equipment can operate at high frequencies, reducing the size and weight of transformers used in the AC portions of the system.
- Electromagnetic interference concerns are reduced compared to AC and HFAC systems.
- Cable weights may be reduced slightly due to elimination of the reactive component of impedance and skin effect.
- Fault current may be interrupted at lower values through the use of power electronics.
- Acoustic performance of the power system can be improved by operating equip-

ment over a range of speeds or frequencies, resulting in a broader signal.

- Adding power sources to a bus only requires adjusting voltage.
- Higher-demand mission loads can be served using a denser architecture.

1.3 Problem to Solve

While there are many advantages to be realized by moving to DC electrical distribution systems, there are still a number of challenges to overcome [10]. The first challenge identified is

> Traditional fault detection and isolation techniques employed by conventional circuit breakers and based on fault current are not desirable for MVDC systems due to the difficulty in extinguishing DC arcs in the absence of a voltage or current zero crossing. Instead, MVDC is anticipated to use power electronics and advanced controls to quickly identify and isolate faults before large fault currents are generated. In the design of the power electronics, consideration must be made to ensure transient stability and limit potential over-voltages during transients. The details, methods, and standards for implementing a power electronics and advanced controls based fault detection and isolation require research and development in addition to implementation engineering. Additionally, new fault detection and isolation components may need to be developed.

Progress has been made in some areas, such as the development of the z-source circuit breaker [13], but integration of the available technologies for a naval application is far from complete. This thesis will examine exiting technologies and then focus on the suitability of the z-source circuit breaker for use in future MVDC naval power systems.

THIS PAGE INTENTIONALLY LEFT BLANK

Chapter 2

Existing Types of Circuit Protection Equipment

Using currently available technology on an AC shipboard system there are a number of way to interrupt current in the event of a fault condition. These technologies include:

- Mechanical circuit breakers
- Fuses
- Relays and controllers
- Power conversion modules

Some of these technologies can be directly transferred to DC systems at low voltage levels, but at medium voltage levels they do not work well or at all, while some can be used across a wide range of voltages.

2.1 Mechanical Circuit Breakers

Circuit breakers are the predominant type of protective device found in naval electrical distribution systems today. These devices work well in both AC systems and lower power DC systems, and can be setup in a way that a given load or location in the system is protected by multiple circuit breakers using what is called selective tripping [12], [14]. Selective tripping also protects the system while de-energizing the

smallest section required to isolate the fault. Circuit breakers are a useful form of protection because they can be reset after they actuate. They can be permanently installed in a system and reused over and over.

Mechanical circuit breakers interrupt a fault current by physically separating a pair of contacts and opening an electrical circuit. For lower power systems, the resistance inserted into the system by the air gap is enough to stop the flow of current. When the separation of the air gap alone is not sufficient the air will ionize and continue to conduct current. In this case other mechanisms in the circuit breaker, such as arc chutes, magnetic guides, and blasts of compressed gases, help extinguish any arc that may form. Some circuit breakers also operate in a vacuum so there is no material between the contacts to ionize. Power electronics can also be used to accomplish the same functionality with solid-state components by opening the switch (e.g. a transistor or thyristor). The amount of current that can be interrupted is ultimately limited by how far apart the contacts can be moved. Circuit breakers can interrupt a larger RMS value for AC current than DC current because of the periodic properties of an alternating current. The periodic zero crossings mean that, in a 60 Hz system, the current will momentarily be zero 120 times per second, significantly reducing the current that the device has to interrupt. To achieve a similar level of current interruption capacity, DC circuit breakers must be designed differently because there is no natural zero-crossing. The physical separation of the contacts required in an MVDC device to arrest arcing is excessive, requiring larger devices and longer opening times. A typical naval MVAC circuit breaker, such as the Eaton 75VCP-W500, opens in 30 to 45 milliseconds from the time a trip command is initiated [15].

Circuit breakers used in naval power systems can be tripped automatically for a number of abnormal conditions. Many circuit breakers have integral magnetic trip mechanisms that provide instantaneous overcurrent protection and some smaller units have bimetallic thermal elements that act as variable-time-current-dependent overcurrent trip mechanisms. Mechanical circuit breakers can be designed without integral mechanisms, though, and rely purely on external protective relays to actuate the circuit breaker. Some MVAC naval circuit breakers, such as the Eaton 75VCP-

W500 utilized on USCGC *Healy* (WAGB 20) [16], rely exclusively on external relays to trip the circuit breaker.

2.2 Fuses

Fuses, or fusible links, also feature prominently in current naval power systems. Like mechanical circuit breakers, fuses are suitable for use in AC systems and lower power DC systems. Fuses are usually used for lower-powered, non-vital loads or as a backup protective device. IEEE recommends against using fuses to protect main buses in an MVDC system [17].

Fuses interrupt a fault current by heating the fuse element to the point that it melts if the current flowing through it exceeds the device's set point. The melting element opens the electrical circuit. If the fuse is properly sized then a large enough gap is created to interrupt the flow of current without a sustained arc forming. The size of the gap created by the melting fuse element determines the fault interrupting capacity by its ability to extinguish any arc that may initially form. The fuse element can be surrounded by a quenching fluid to increase its interrupting capability without increasing its size. As in the mechanical circuit breaker, fuses can interrupt larger RMS currents in an AC system than in a DC system because of the periodic zero-crossing. Fuses for AC systems are readily available at ratings greater than 100 kV while fuses for DC systems are commercially available only into the lower end of the medium voltage range, up to around 4 kV.

2.3 Relays and Controllers

Relays, or any form of motor controller, can also function as protective devices. These devices tend to be used to protect the load from damage in the event of abnormal power system conditions, such as when a pump is automatically stopped because the voltage or frequency of its AC supply becomes too low for safe operation. This is in contrast to the type of protection provided by circuit breakers and fuses, which

are generally meant to protect the power system from damage. Relays tend to be sized to interrupt normal operating, whereas circuit breakers and fuses are meant to interrupt larger fault currents. This limits their usefulness in overall power system protection schemes.

2.4 Power Conversion Modules

Power conversion modules (PCMs), especially switching converters, can provide protective functionality in addition to their normal functions of voltage or current regulation. A switching converter has at least one actively controlled switch, such as a transistor or gate turn-off thyristor, that can be positioned on or off to reduce the PCM's output power to zero. Driving the PCM's output to zero can be used to de-energize the faulted circuit if the PCM has the proper sensors and control algorithms to detect fault conditions. At the laboratory bench scale some power supplies have a built-in capability to do this, such as the Matsusada Precision RE500-2.4 used in the experimental setup discussed in Chapter 4, while some lack the capability to sense a fault, as is the case with the Hewlett Packard 6010A also used in the experimental setup. Using the PCM to de-energize a fault can be very fast. A PCM with characteristics similar to one that might be found in a future naval MVDC power system is used in the Florida State University Center for Advanced Power Systems. This converter operates with an effective switching frequency of 2 kHz [18]. If the PCM takes ten cycles to drive its output to zero it would have a de-energization time of 5 milliseconds, much faster than typical large circuit breaker.

Chapter 3

The Z-source Circuit Breaker

The z-source circuit breaker is a solid-state DC circuit breaker that controls current flow with a thyristor. The circuit breaker was initially developed by Corzine and Ashton in 2010 [13]. The topology was inspired by the z-source inverter developed by Peng [19]. The original z-source circuit breaker configuration is shown in Figure 3-1. Variations of the original topology (crossed) have been developed, including the parallel-connected [20] and series-connected [21] configurations. These three configurations only support unidirectional current flow. Other derivations have been proposed that support bidirectional current flow [22], [23], [24], and [25].

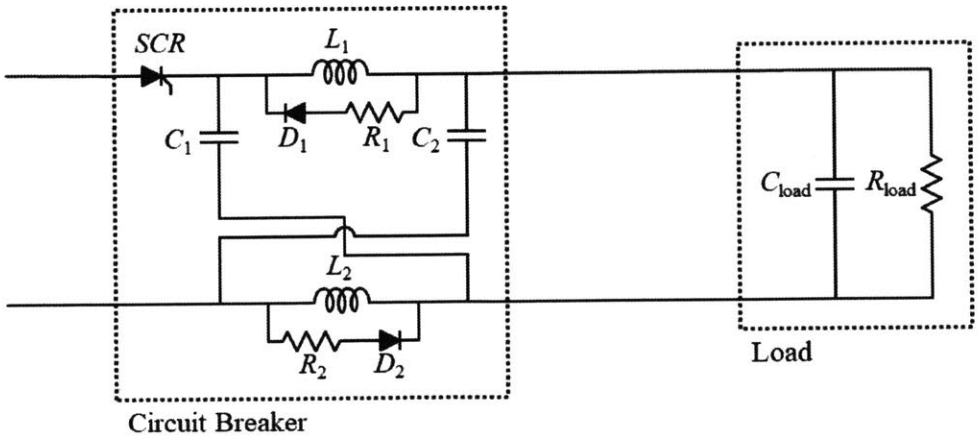

Figure 3-1. The initial z-source circuit breaker topology proposed by Corzine and Ashton [13].

Chang et al. compared the advantages and disadvantages of crossed, parallel-connected, and series-connected topologies [21]. Based on those comparisons, summarized in Table 3.1, the series-connected topology is the most suitable for use in a naval power system due to the common ground and the minimal fault current seen at the source. This topology, shown in Figure 3-2, will be the focus of discussion from here on out.

Table 3.1. Z-source Circuit Breaker Topology Comparison [21].

Features	**Topology**		
	Crossed	**Parallel**	**Series**
Common Ground	No	Yes	Yes
Fault Current at Source	I_{SCR}	$I_L + I_C$	I_L
Transfer Function	Resonator	Notch Filter	Low-pass
Input Filter Integration	No	No	Yes

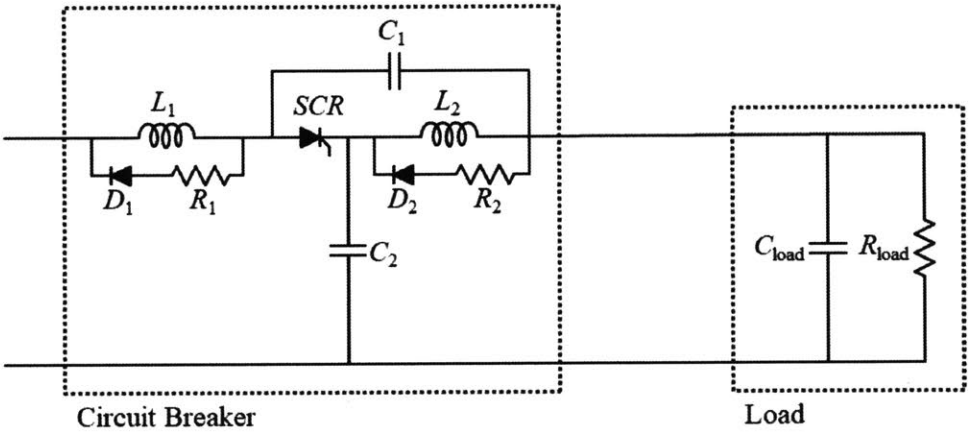

Figure 3-2. The series-connected variation of the z-source circuit breaker developed at MIT by Chang et al. [21].

3.1 Circuit Operation

For this research circuit breaker operation was simulated in LTSpice XVII and confirmed using an electrically-scaled model. Details of the LTSpice model are given in Appendix B and the development of the scale model is discussed in detail in

Appendices C and D. The circuit's operation can be divided into four phases: off-state, turn-on, on-state, and fault.

Initially the circuit breaker is in the off-state. It appears as an open circuit in the power system because the thyristor is in forward blocking mode. The anode of the thyristor is at the source voltage and the cathode is at ground. The capacitor in parallel with the thyristor, C_1, is charged to the source voltage.

The turn-on phase is a transient condition that lasts for only a few milliseconds. When the thyristor is gated on current begins to flow through the thyristor and it enters forward conducting mode. During the turn-on transient inductors L_1 and L_2 initially resist the change in current, causing the voltage at the thyristor's anode to dip slightly. Capacitor C_1 discharges to approximately zero and capacitor C_2 charges to approximately the source voltage. The thyristor's anode and cathode voltages both stabilize at approximately the source voltage. There may be additional transients during turn-on that occur as voltage is initially applied to the load, depending on its impedance, i.e. the circuit may exhibit additional ringing transients if an inductive component is added to the load. Figure 3-3 illustrates these transients as simulated in LTSpice and Figure 3-4 shows actual transients recorded on the scale model. These transients do not match as well as may be desired, but the goal for this simulation was to accurately model fault transients. The transient in the simulation stretches over a longer period of time than in the scale model and the peak current is lower than in the scale scale model. These discrepancies are likely a result of the change in load resistance that occurs as the light bulb filament of the load warms and its resistance increases.

Once the turn-on transient is over the circuit breaker enters the on-state condition. In steady-state operation current flows from the source, through the thyristor, to the load. If ideal components are used there are no losses in the circuit breaker. In a real implementation of the circuit losses will arise in the inductors and the thyristor, but the power dissipation is minimal compared to the power delivered to the load. Capacitor C_2 remains charged to approximately the source voltage. The circuit, as configured in Figure 3-2, will continue to operate in the steady-state mode until

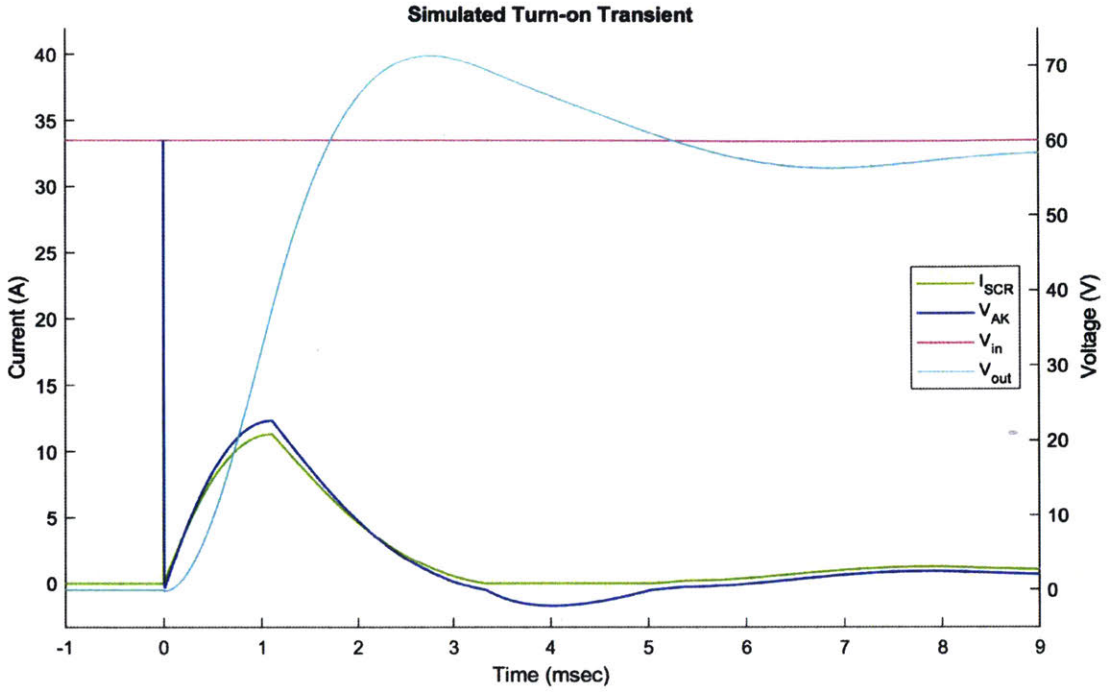

Figure 3-3. Simulated turn-on transients in a series-connected z-source circuit breaker.

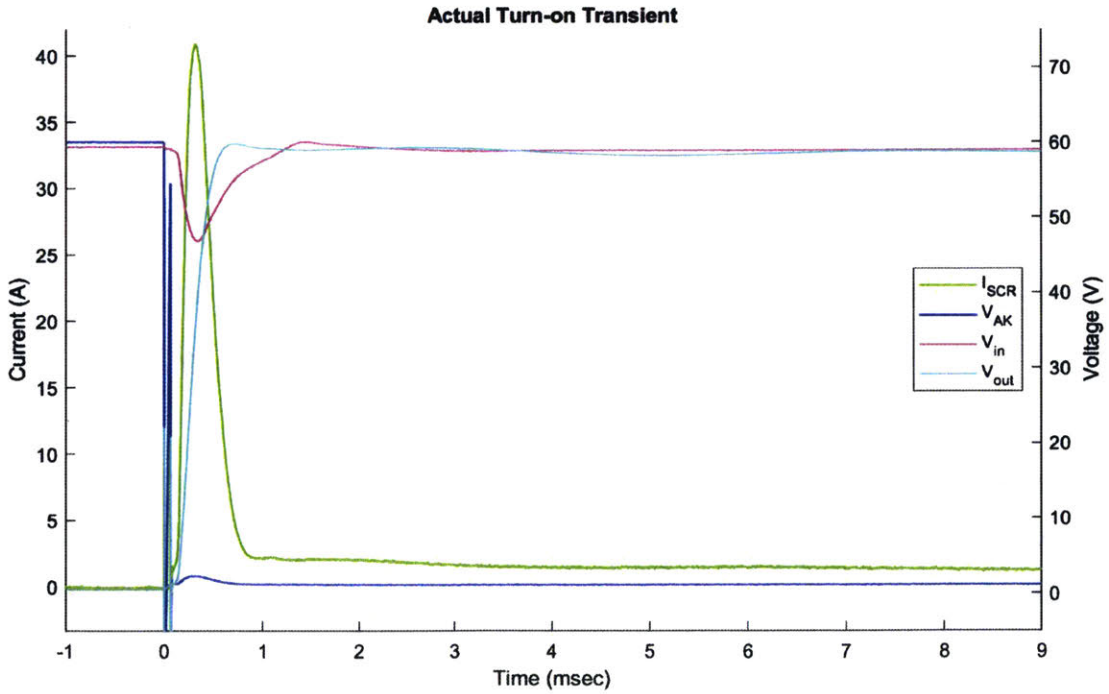

Figure 3-4. Actual turn-on transients measured in the scale-model series-connected z-source circuit breaker.

either a fault occurs on the load side of the circuit breaker or the source voltage is interrupted, i.e. there is no mechanism to turn it off.

The last phase of operation is the fault condition. If a short-circuit fault occurs on the load side of the circuit breaker that creates a sufficiently large $\frac{di}{dt}$, a transient is set in motion that ultimately turns the circuit breaker off. As the fault is inserted the output voltage is pulled to ground. Inductor L_2 opposes the sharp rise in current and prevents the fault current from being supplied though the thyristor. The high-speed transient fault current is supplied by capacitor C_1, causing the voltage at the thyristor's anode to dip lower than the source voltage. Capacitor C_2 maintains the voltage at the thyristor's cathode at approximately the source voltage. This reverse biases the thyristor and it enters reverse blocking mode. Capacitor C_2 charges to approximately source voltage. Any charge stored in the load capacitance is discharged through the fault. The currents in inductors L_1 and L_2 circulate through the diode and resistor snubbers until the stored energy is dissipated. At this point the load bus is completely de-energized. Figure 3-5 illustrates these transients as simulated in LTSpice and Figure 3-6 shows the same transients in the scale model. Data from the simulation and the scale model match well for this transient overall, although the scale model does show a very brief reverse current through the thyristor that is not present in the simulation due to the idealization of the simulated thyristor. Additionally, V_{AK} exhibits some ringing from the interaction between C_1 and L_1 after the current circulating through the dampers decays away.

It is important to point out that this fault interrupting mechanism in the z-source circuit breaker is an intrinsic characteristic of the circuit. Unlike the mechanical circuit breakers used in AC and DC naval electrical distribution systems that require some sort of sensor or internal detection mechanism to detect a fault condition, the z-source circuit breaker inherently responds to a sharp rise in current by turning off. This is comparable to how a fuse's functionality is inherent to its fabrication. The threshold for what constitutes a sharp rise is determined in the selection of the values of C_1, C_2, L_1, and L_2 as discussed in [13] and [21].

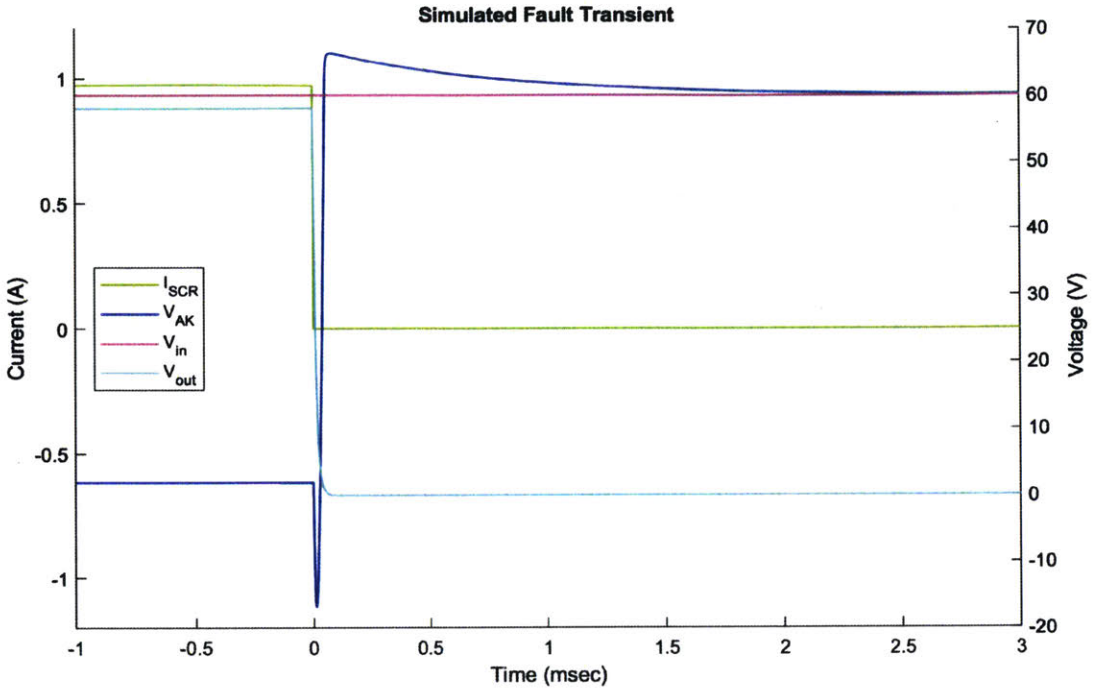

Figure 3-5. Simulated transients in a series-connected z-source circuit breaker for a fault initiated after the system reaches steady-state operation.

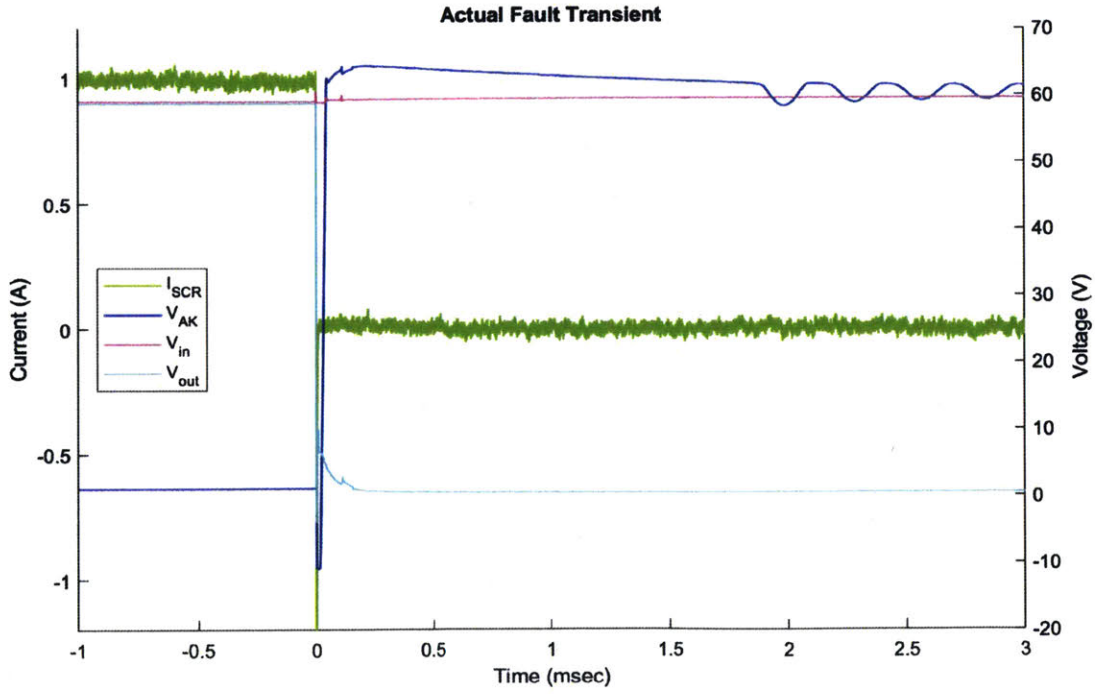

Figure 3-6. Actual transients measured in the caled-model series-connected z-source circuit breaker for a fault initiated after the system reaches steady-state operation.

3.1.1 Controlled Turn-off

If built exactly as shown in Figure 3-2, the circuit breaker has no mechanism by which it can be manually turned off. For the series-connected z-source circuit breaker, Chang et al. discuss two ways that the circuit breaker could be manually turned off [21].

Figure 3-7 shows how a switch and current-limiting resistor could be implemented as an artificial external fault. This mechanism turns off the circuit breaker in the same fashion as the fault turn-off discussed previously. The diode added to the circuit limits the current carried by the artificial fault by blocking the load capacitance from discharging through the artificial fault and reduces the current required to turn off the device from 11 times the nominal load current to just twice the nominal load current [21]. The disadvantage of this topology is the additional power lost through dissipation in the blocking diode.

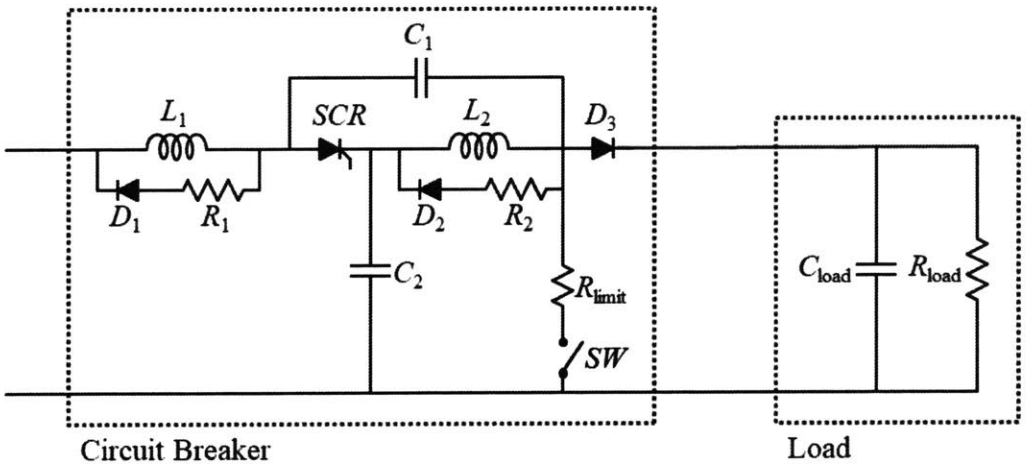

Figure 3-7. A series-connected z-source circuit breaker with a turn-off mechanism on the load side of the thyristor.

Figure 3-8 shows the topology incorporating the internal artificial fault mechanism. The manner in which this topology turns the circuit breaker off is different from the way in which the external fault works. In the internal artificial fault topology, when the off switch is closed the current flowing through the thyristor is diverted

through the off switch circuitry and the voltage at the thyristor's anode is pulled to ground. Capacitor C_2 keeps the voltage at the thyristor's cathode at approximately the source voltage. This reverse biases the thyristor and terminates current flow to the load. The initial current is limited by the series resistor. The capacitor C_{aux} charges during the turn-off transient, gradually bringing the voltage across it to near the source voltage. The parallel resistor limits the switch current at the end of the turn-off transient. If the switch is implemented as a thyristor this resistor should be sized to reduce current to below the holding current, allowing the switch to naturally turn off at the end of the circuit breaker turn-off transient. If the switch is implemented as a transistor then the resistor is sized to limit current at the end of the turn-off transient to a level that can safely be interrupted by the transistor.

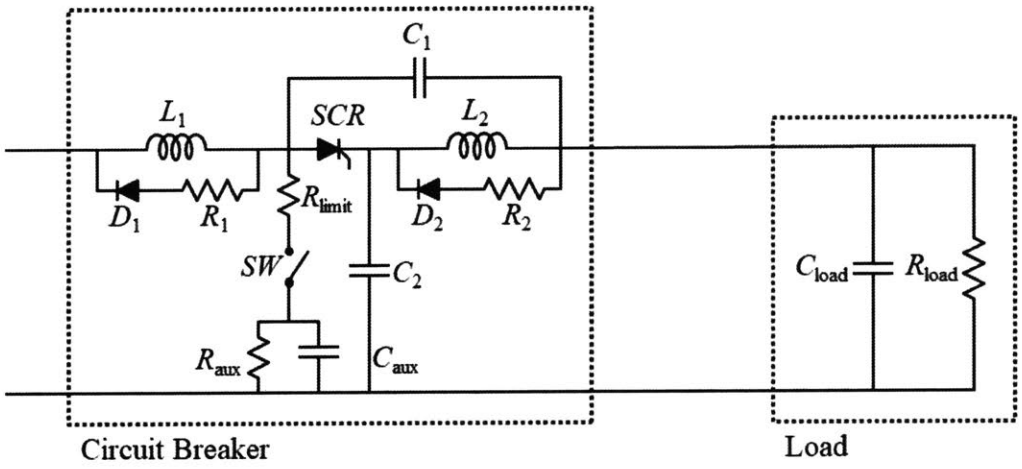

Figure 3-8. A series-connected z-source circuit breaker with a turn-off mechanism on the source side of the thyristor.

Either of these mechanisms allows manual tripping of the circuit breaker. These mechanisms can also be paired with one or more sensors or protective relays to implement automatic trips based on fault conditions other than a sharp rise in current. This allows the z-source circuit breaker to implement trip set points for over-current protection, under-voltage protection, etc. The manual trip mechanism can also be connected to shipboard control systems to allow for remote operation or coordination with other electrical system operations.

3.2 Further Investigation Needed

At this point, z-source circuit breakers are not ready to be used as drop-in replacements for conventional mechanical circuit breakers. Further study and development of some aspects of the z-source circuit breaker are needed.

The first such area is failure mode. The failure modes for a thyristor, the central element of the z-source circuit breaker, are different from those of a mechanical switch used in a conventional circuit breaker. Two well-known failure modes, perhaps more appropriately described as false triggering mechanisms, for thyristors could impact circuit breaker design and integration of the circuit breaker into the larger power system. The first is break-over, in which the thyristor is turned on by applying too high of a voltage across the device [26]. In this case the V_{BO} rating is violated. While this turn-on mode may be useful in some applications, it is undesirable in a circuit breaker where the gate pulse is expected to control turn-on behavior. The second is pushing the thyristor into regenerative turn-on mode by applying a sufficiently large positive change in forward voltage across the device [26]. In this case the $\frac{dV_{AK}}{dt}$ rating is violated. The initial focus for research was in quantifying $\frac{dV_{AK}}{dt}$ during tripping transients in a model system that is representative of a naval power system.

The second area where further research should be conducted is faults during transient conditions. A review of the literature, for example [13], [20], [21], and [23], shows that the analyses of tripping transients are all conducted with the circuit breaker initially starting at some steady-state operating point. The circuit breaker's fault isolation behavior during a turn-on transient must be better understood prior to deployment in operational power systems. After a fortuitous equipment failure during the first few tests to quantify $\frac{dV_{AK}}{dt}$, understanding fault isolation capabilities when not starting from steady-state became the other focus of this research.

A third area warranting attention is the control system, specifically the gating pulses used to turn the circuit breaker on, or maintain it on during very low current flow conditions. The gating signal is initially required to initiate current flow through the thyristor, but it may also need to be reapplied periodically as well. The trouble

with this approach, independent of the pulse frequency used, is that if the control system is unaware of a faulted condition, due to either inadequate sensor input or a time delay between detecting a fault condition and inhibiting the periodic gating signal, the circuit breaker may be re-closed on a fault and it will be unable to re-break as will be discussed in Chapter 5. Coordination amongst sensors and the control system will need to be more tightly integrated than in current naval power systems to ensure low latency.

Chapter 4

Quantifying $\frac{dV_{AK}}{dt}$ During Tripping Transients

4.1 Motivation

One method to turn on a thyristor, aside from the normal method of applying an appropriate signal to the gate terminal, is pushing the thyristor into regenerative turn-on mode by applying a sufficiently large positive change in forward voltage across the device [26]. Many thyristors have a $\frac{dV_{AK}}{dt}$ rating, and it must be observed to prevent this type of unintended turn-on.

In many power systems, transmission and distribution line impedances tend to be dominated by inductance [27]. A sudden change in the current flowing through the circuit, like the transient that occurs when a circuit breaker trips, can cause a spike in voltage across an inductor, a phenomenon sometimes referred to as "inductive kick." Naval power systems have relatively short cables compared to terrestrial systems and their impedances tend to be dominated by resistance, so inductive kick may not be as large of a concern on a ship. However, the current in a z-source circuit breaker flows through inductors on both sides of the thyristor meaning that inductive kick still may be a consideration in a naval MVDC system. Also, some the loads supplied by the power system may be inductive in nature so it is necessary to understand how the z-source circuit breaker will respond in an inductive system. Previous research

has focused on operation of the z-source circuit breaker and how it isolated a fault in a system, for example [13], [20], [21], and [23]. The loads in these studies also tended to be composed of only capacitive and resistive elements. There was no discussion regarding how well the systems in these tests represented naval power systems. Of particular interest is how well the cables between the power source and the circuit breaker match shipboard cables.

This chapter will focus on quantifying what a "typical" naval MVDC power system is and how the voltage transients within a series-connected z-source circuit breaker behave. Understanding the voltage transients will help inform component selection for full-scale circuit breakers and determine what, if any, snubbers should be included.

4.2 Typical Naval MVDC Power System

Defining a "typical" naval MVDC system is difficult because no such systems have been designed or placed in operation yet. In the U.S. Navy all shipboard electrical distribution systems are low voltage AC or DC, or medium voltage AC. Some studies have examined appropriate components for use in a shipboard MVDC system in an effort to model those systems for concept-level designs [28]. The data from this effort was used to estimate the "typical" properties for cables listed in Table 4.1. Additionally, some components that may be included in an MVDC system, such as cable, have been specified for projects currently in production but not yet placed in operation, such as the 1000 VDC link that powers the new Air and Missile Defense Radar (AN/SPY-6) that is being installed on the Flight III *Arleigh Burke*-class guided missile destroyers [29]. Others have studied the loads that may be found on an MVDC distribution system, such as Power Conversion Modules (PCM)[1] [18]. A group at the Florida State University operates the Center for Advanced Power Systems. Chauncey studied and characterized one of their Modular Multilevel Converters, essentially a PCM, that is one of the best available representations of what will be used in the

[1]PCMs generically convert power from one form to a different form. In this context they are generally solid-state switching converters used for DC-to-DC or DC-to-AC conversion.

near future in naval MVDC power systems. This information was used to estimate the "typical" PCM properties shown in Table 4.2. Doerry and Amy suggest different MVDC distribution standard voltages of 6 kV, 12 kV, and 18 kV that may also represent typical system parameters [30]. Together, these sources give the best representation of naval MVDC power system components available in open literature.

Table 4.1. Typical MVDC cable characteristics.

Property	Value
Resistance	47.00 μΩ/m
Capacitance	561.00 pF/m
Inductance	490.00 nH/m
Characteristic Impedance	29.6 Ω

Table 4.2. Typical MVDC PCM characteristics.

Property	Value
Power	1 MW
Voltage	6000 VDC
Resistance	36.0 Ω
Capacitance	364 μF

4.3 Experimental Setup

The experimental setup emulates the typical naval MVDC system parameters developed above. Laboratory resources limit the voltages that can be studied, so a scaled model must be used for measurements. This model will uses per-unit scaling and is developed in detail in Appendices C and D. The characteristics of the full-scale and model-scale power systems are summarized in Table 4.3. The model was intentionally scaled in such a way that time parameters in both the full-scale and model-scale systems are equal. There were several modeling issues encountered that led to multiple redesign cycles that are also detailed in Appendix D and later in this chapter. The model consists of a power supply, a z-source circuit breaker, a load, interconnecting cables, and a fault insertion device. The model-scale power system is

shown in Figure 4-1. The laboratory equipment used in this setup is listed in Table 4.4.

Table 4.3. Full-scale and model-scale power system characteristics.

System	Full-scale	Per-unit	Model-scale
V_{source}	6000 VDC	1.000	60.0 VDC
P_{load}	1 MW	0.821	59.1 W
I_{load}	166.7 A	0.821	0.985 A
R_{load}	36.0 Ω	1.218	60.9 Ω
C_{load}	364 µF	N/A	215 µF
$\lvert Z_{0,\text{ line}}\rvert$	29.6 Ω	1.0000	50.0 Ω

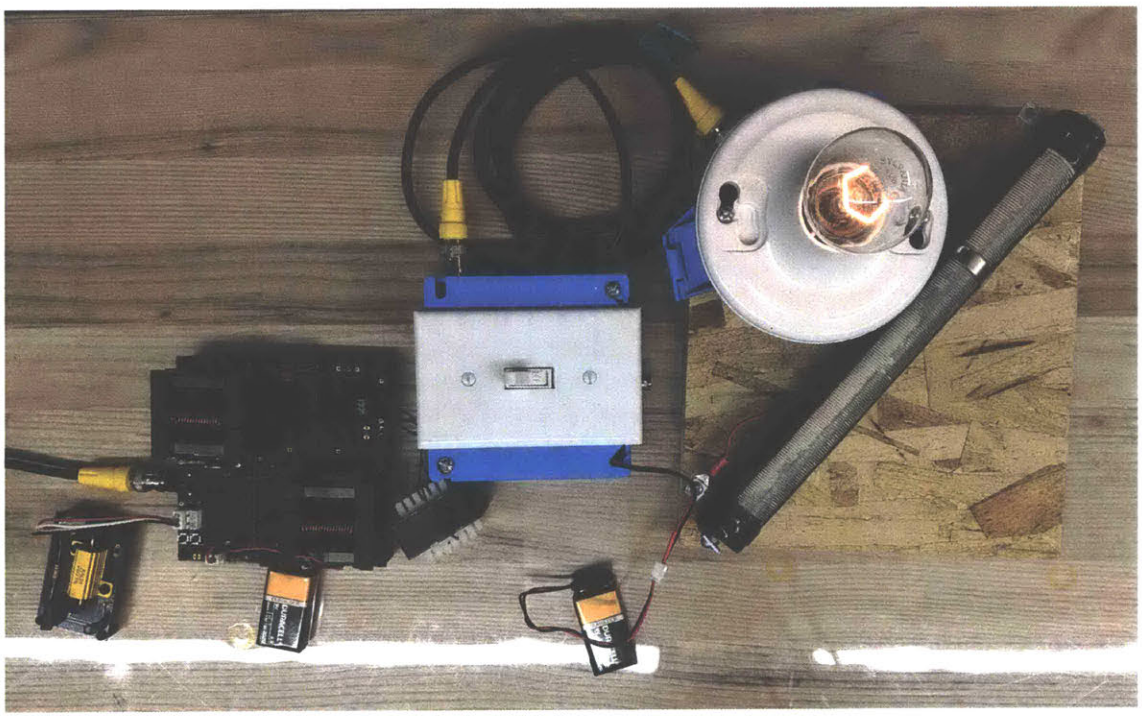

Figure 4-1. The model-scale power system used in the experiments.

Table 4.4. Equipment used in the experimental setup.

Component	Manufacturer	Model	Serial Number
DC power supply	Matsusada Precision	RE500-2.4-LUs1	058616S
DC power supply	Hewlett Packard	6010A	3214A-01196
LCR/ESR Meter	BK Precision	889A	35104070098
Oscilloscope	Tektronix	MDO3034	C018851
Current probe	Tektronix	TCP0030A	C004143
Current probe	Tektronix	TCP0030A	CC04171
Diff. voltage probe	Tektronix	THDP0200	C022079
Diff. voltage probe	Tektronix	THDP0200	C022300
Diff. voltage probe	Tektronix	THDP0200	C022301

4.4 Experimental Method

The goal of each test was to collect data for V_{AK} during a fault transient. The circuit breaker's input voltage, V_{in}, output voltage, V_{out}, and thyristor current, I_{SCR} were also collected to verify proper operation during each test. Table 4.5 lists where each probe was connected on the circuit to collect measurements and Figure 4-2 shows the quantities measured on the simplified circuit diagram. Once the circuit was proven functional there were four sets of tests run to collect data. For each set of tests a different value of L_{added} was used to determine its effect on the voltage transients. The four values used were 0 µH, 23.8 µH, 44.7 µH, and 107 µH. These inductance values were selected because of inductor availability. The tests conducted with no additional added inductance serve as the baseline for comparison for the other three sets of tests, and to validate that there were no unexpected transients occurring in the circuit that might affect the other data collected. These tests also confirmed that the characteristic impedance of the cable alone did not produce large voltage transients. Figure 4-3 shows a test conducted as part of the set with no added inductance. The signal of interest for testing is shown in dark blue, signal 1.

Initial setup consisted of connecting the oscilloscope probes to the circuit and configuring the display and data collection setting. The power supply was energized and allowed to warm up for at least five minutes. The circuit breaker was turned on and off several times to verify the expected response was observed on the oscilloscope

Table 4.5. Test points for data collection.

Measurement	Test Point 1	Test Point 2	Channel
V_{AK}	TP-V2 (-)	TP-V3 (+)	1
V_{out}	TP-V8 (-)	TP-V7 (+)	2
V_{in}	TP-V9 (-)	TP-V1 (+)	3
I_{SCR}	TP-I3 (clamp)	TP-GND (ground)	4

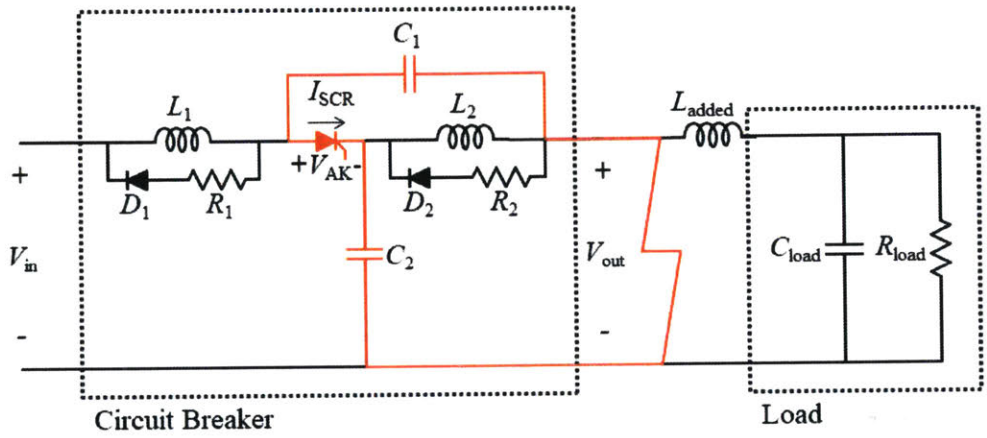

Figure 4-2. Quantities measured during each experiment.

and that the triggering settings worked as desired.

For each test the load was energized using switch SW1 on the circuit breaker and allowed to warm-up. The warm-up is necessary to allow the load to stabilize as the light bulb filament settles to its operating temperature and steady-state resistance. After a sufficient warm-up the switch on the fault insertion device was thrown to create the required short circuit. The oscilloscope data was visually verified to confirm the fault was inserted correctly and the full data set saved to a USB flash drive. The data was transferred to a computer for detailed analysis in MATLAB R2017b.

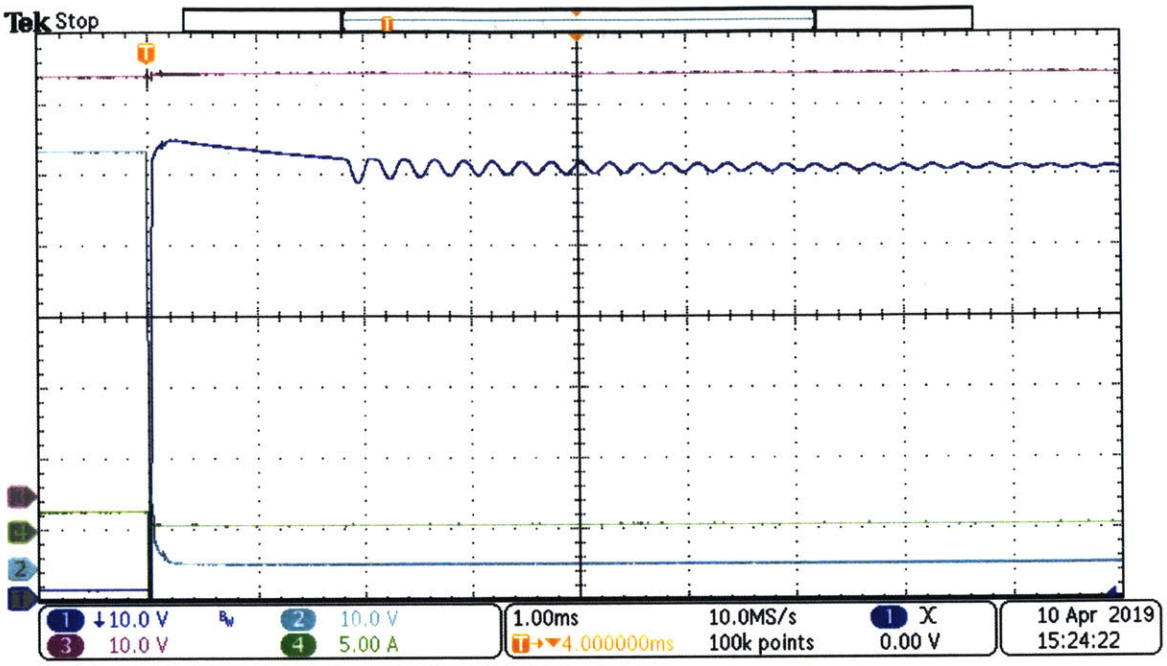

Figure 4-3. Typical fault transient traces for a system with no added inductance. Signal 1 is V_{AK}, 2 is V_{out}, 3 is V_{in}, and 4 is I_{SCR}.

4.5 Results

None of the observed fault turn-off transients produced sufficiently high values of $\frac{dV_{AK}}{dt}$ to force the thyristor into regenerative turn-on mode. This means that the thyristor should not be contributing any anomalies to the measurement of V_{AK} in these experiments.

In the tests where $L_{added} = 0$ there was ringing observed in V_{AK} starting about 2 milliseconds after the fault insertion and damping out several milliseconds later. The frequency of this ringing corresponds to an LC circuit composed of C_1 and L_1. The onset of the ringing is delayed as the current flowing in L_1 at the time of fault initiation takes time to decay through the diode-resistor snubber to the point that the inductor can ring with the capacitor. The $\frac{dV_{AK}}{dt}$ is low and is not the information sought in these experiments.

In the other three sets of tests there were additional ringing transients observed in both V_{AK} and V_{out} during the first millisecond after the fault insertion. Figure 4-4 shows the traces from a test with $L_{added} = 107\ \mu H$, where the additional ringing is

most pronounced. The ringing in V_{AK} and V_{out} have the same frequency and appear to be caused by the same phenomenon. In the case of Figure 4-4 the frequency of oscillation matches that caused by a 107 µH inductance and a 1.19 µF capacitance. The inductance can be easily accounted for by L_{added} and, at first examination, the capacitance is close to that of C_1 or C_2. The ringing cannot come from C_2, though, because the inductance from L_2 would also have to be involved. The ringing also cannot come solely from C_1 because the energy is dissipated relatively fast and an LC circuit comprised of C_1 and L_{added} has no element in which to dissipate the energy. Noting that the capacitance involved is not an exact match to C_1 and that the energy is quickly dissipated, the load elements are likely candidates for involvement in this ringing transient. The series combination of C_1 and C_{load} is 1.193 µF and matches capacitance calculated from the ringing oscillations. These ringing transients are caused by an RLC circuit comprised of R_{load}, L_{added}, C_1, and C_{load} arranged as shown in Figure 4-5. Figure 4-6 shows how this ringing varies as L_{added} is increased. The plot for $L_{added} = 23.8\ \mu H$ is offset by 0.5 milliseconds, the plot for $L_{added} = 44.7\ \mu H$ is offset by 1.0 milliseconds, and the plot for $L_{added} = 107\ \mu H$ is offset by 1.5 milliseconds. This transient is what needs to be characterized in these experiments.

The part of this transient that is of interest is the part of the signal where voltage increases most rapidly. This is the first rise in voltage after the peak and initial fall in all of the cases measured. The slope of this curve was measured and the results compiled in Table 4.6. These results are scaled back to full-scale values in Table 4.7 to show what is predicted to occur in a typical naval MVDC power system.

Table 4.6. Voltage transient results.

L_{added}	Maximum $\frac{dV_{AK}}{dt}$		
	Minimum	**Mean**	**Maximum**
23.8 µH	0.454 V/µs	0.485 V/µs	0.513 V/µs
44.7 µH	0.547 V/µs	0.579 V/µs	0.610 V/µs
107 µH	0.790 V/µs	0.863 V/µs	0.968 V/µs

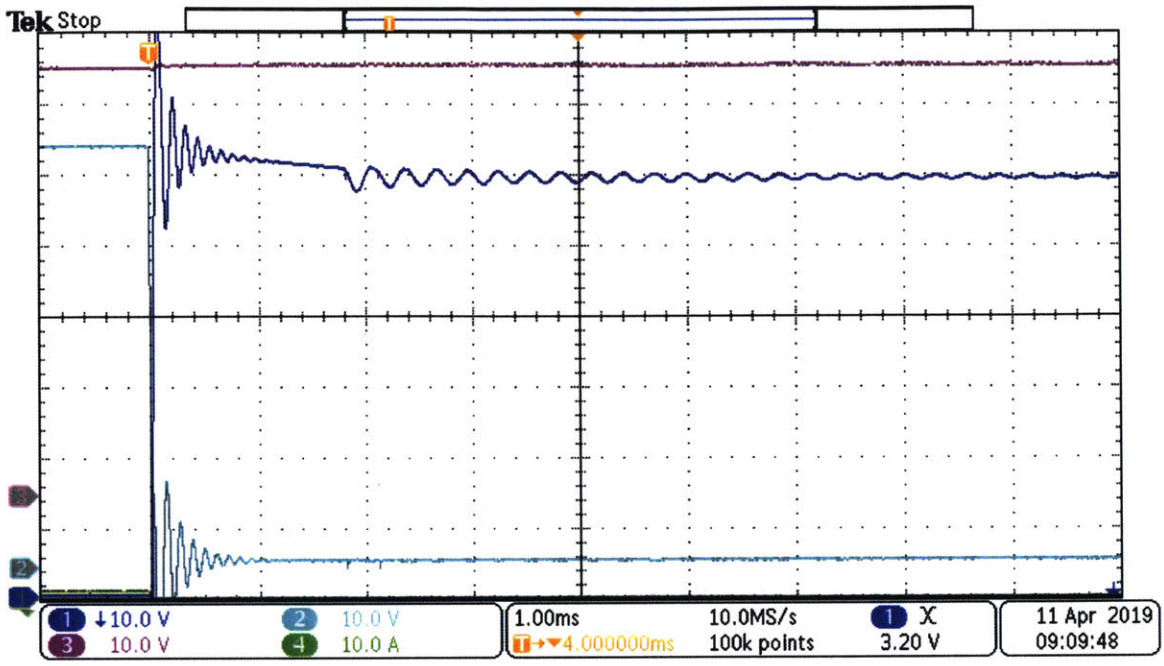

Figure 4-4. Typical fault transient traces for a system with $L_{added} = 107\ \mu H$. Signal 1 is V_{AK}, 2 is V_{out}, 3 is V_{in}, and 4 is I_{SCR}.

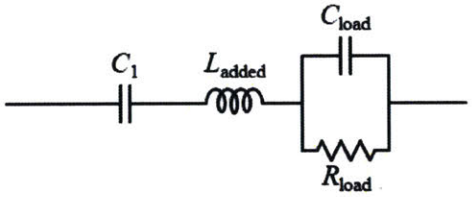

Figure 4-5. The RLC oscillator responsible for the first ringing transient shown in Figure 4-4.

Table 4.7. Model-scale results and full-scale predictions.

Model scale		**Full scale**	
$\mathbf{L_{added}}$	$\frac{dV_{AK}}{dt}$	$\mathbf{L_{added}}$	$\frac{dV_{AK}}{dt}$
23.8 µH	0.485 V/µs	237 µH	48.5 V/µs
44.7 µH	0.579 V/µs	445 µH	57.9 V/µs
107 µH	0.863 V/µs	1.06 mH	86.3 V/µs

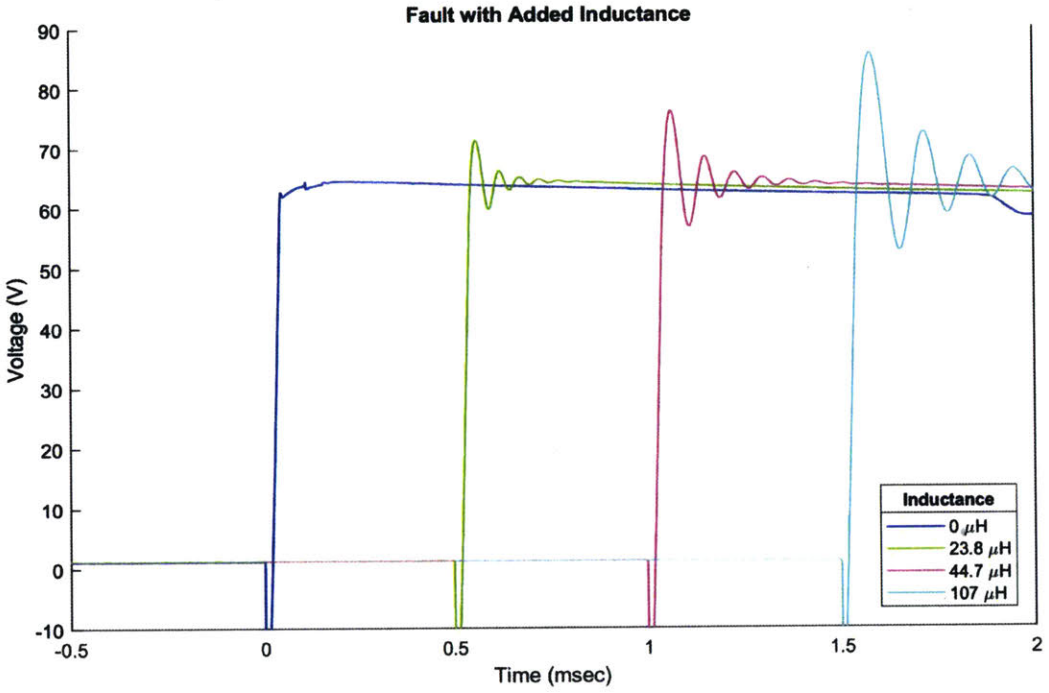

Figure 4-6. Results of testing showing how the amplitude of the the V_{AK} transient varies as L_{added} is varied. For clarity, this plot shows the transients offset by 0.5 milliseconds.

4.6 Experimental Difficulties

There were many modifications required to get the experimental setup functioning correctly and into a configuration that facilitated data collection. These difficulties resulted from underestimating or altogether failing to account for parasitic characteristics and other non-idealities present in a real-world circuit.

4.6.1 Power Supply Protective Action

The first difficulty encountered was that the DC power supply (Matsusada Precision RE500-2.4-LUs1) entered a protective mode when the fault in the test system was initiated. The power supply detected a short circuit on its output and briefly stopped switching until the fault was cleared. Casual observation of this transient could be, and was initially, wrongly interpreted as the circuit breaker functioning correctly because it occurred on a time scale of milliseconds. Figure 4-7 shows this transient as displayed on the oscilloscope. Trace 1 is the voltage across the thyristor and trace 2 is the circuit breaker input voltage, which is effectively the same as the power supply output voltage. Trace 4 is a control signal that was used for fault insertion and oscilloscope triggering, and can be ignored. Prior to insertion of the short-circuit fault the voltage across the thyristor is approximately 1 V and the input voltage is approximately 60 V. When the fault is inserted the input voltage falls to zero over approximately 2.5 milliseconds. Once the input voltage reaches zero current flow through the thyristor ceases and the voltage across it also falls to zero. This turns off the thyristor, and, after approximately 5 milliseconds, the power supply senses that the fault has cleared. Input voltage ramps back to 60 V over 8 milliseconds but the fault remains isolated.

Extensive troubleshooting determined that the resistance in the fault circuit, shown in red in Figure 4-8, was too high. This limited $\frac{di}{dt}$ to a value that was insufficient to initiate a protective action. The power supply was able to detect the fault *through* the circuit breaker at this point and triggered an unintended protective action. In the end the power supply behavior was not the problem but was merely

an indication of problems with the circuit breaker.

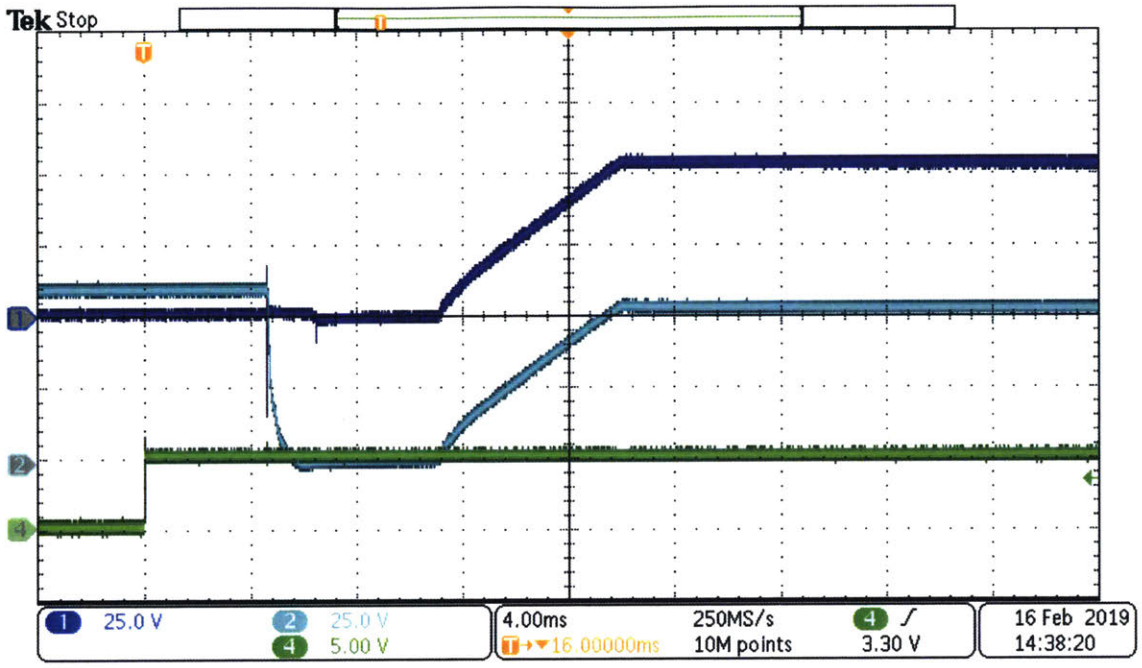

Figure 4-7. Oscilloscope screen image showing the power supply entering and leaving a protective mode.

The fault conductance chosen during the initial iteration of design proved to be too optimistic. Achieving the required fault resistance of 33 mΩ was not possible using the connectors, cables, and circuit board traces in the original scale model. A more realistic value for fault resistance of 100 mΩ was selected and a fault conductance of 10.0 S was specified for the model. This change broke some of the scaling originally designed into the circuit, but this departure does not affect the circuit dynamics which were the driving factor behind the scaling method. Changing the fault characteristics required specifying new capacitors and inductors so protective action would be triggered at the proper $\frac{di}{dt}$. The changes and the supporting calculations are detailed in Appendix D. None of the changes affected the system properties given in Table 4.3, so proper scaling of the overall scale model was preserved.

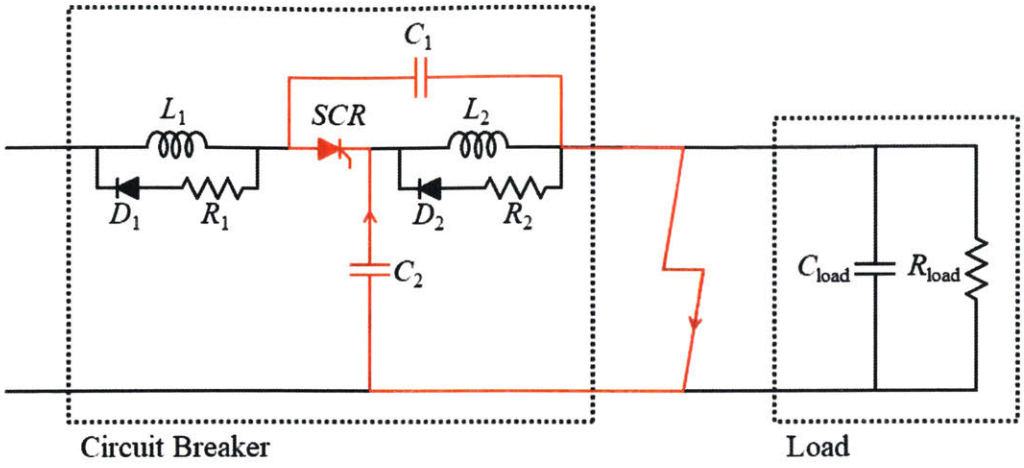

Figure 4-8. Circuit diagram illustrating the path for fault current.

4.6.2 Thyristor Speed

Changing the inductors and capacitors did not correct the circuit breaker's operation, although it was a necessary step to achieving proper operation. The thyristor that was selected in the initial design iteration also proved problematic. The new passive components allowed momentary reverse current in the thyristor that initiated the turn-off process, but did not maintain the conditions long enough for the thyristor to completely turn off, i.e. the zero/reverse current conditions lasted for a duration less than t_q. Once capacitor C_2 was discharged the transient reverse current flow stopped. Since the thyristor had not completely turned off, forward current was again able to flow and the fault was not isolated. Replacing the original thyristor with a device having a shorter turn-off time finally led to proper circuit breaker operation and enabled the collection of the data used in this chapter.

The model-scale system was scaled in a way that the timing requirements observed in this experiment translate directly to the full-scale system requirements. The thyristor that was used in the final design has a very short turn-off time of 25 microseconds. A turn-off time of 110 microseconds proved to be too long. Capacitor C_2 would have to be larger to sustain a reverse current through the thyristor long enough for it to complete the reverse recovery process. Ultimately, an analytical solution is needed to

determine the length of time that reverse current flows through the thyristor during the tripping transient.

4.7 Conclusion

This series of tests gives a starting point for full-scale system design which, combined with computer-based simulation, can aid in component selection. A survey of medium voltage (6 kV to 9 kV) thyristor modules available at Digi-Key Electronics showed that the predicted values for $\frac{dV_{AK}}{dt}$ are significantly lower than the maximum allowable values for full-scale components. These limits ranged from 1000 V/µs to 2000 V/µs, or more than an order of magnitude larger than the values predicted here. Voltage rise rate as a result of tripping transients should not pose a problem for incorporating z-source circuit breakers into future naval power systems.

Chapter 5

Shipboard Power System Integration

5.1 Motivation

As alluded to in Chapter 3, fault handling during major power system transients should be examined as the z-source breaker concept matures. The various forms of the z-source circuit breaker have been shown to provide protection from a rapid rise in current once the circuit breaker circuitry has settled to steady-state, specifically that the shunt capacitors are charged and the parallel capacitors are discharged. This occurs on the order of milliseconds in both the model power system and in LTSpice simulations. This should occur on the order of milliseconds in a full scale power system as well, based on the way the model system was scaled. The manual tripping mechanisms developed in Chang et al. allow the circuit breaker to be tripped after this point for whatever reason may be deemed necessary (e.g. long-term over-current, under-voltage, differential, etc.). A key aspect of circuit operation that has not been covered in detail for the crossed or series-connected topologies is that these trips rely on the shunt capacitors being charged. In a similar way, the parallel-connected topology relies on the parallel capacitors to be discharged at the start of the fault transient. This requirement directly affects the circuit breaker's ability to open, either for a fault or a manual trip, during the initial turn-on transient.

While conducting initial testing to quantify the $\frac{dV_{AK}}{dt}$ in the representative system, an equipment failure led to a test where the circuit breaker was closed on a faulted

output bus, connecting a short-circuited bus to the power supply. The power supply immediately entered current-limiting mode the output voltage dropped. Investigation of this irregularity led to the conclusion that during the previous test the contacts of the relay used to insert the short-circuit fault had somehow become jammed or welded in the closed position[1]. Figure 5-1 shows the damaged relay with its cover removed. The contacts shown are normally open contacts and the relay is de-energized. The contact on the left is stuck in the closed position which created a permanent short circuit in the experimental setup.

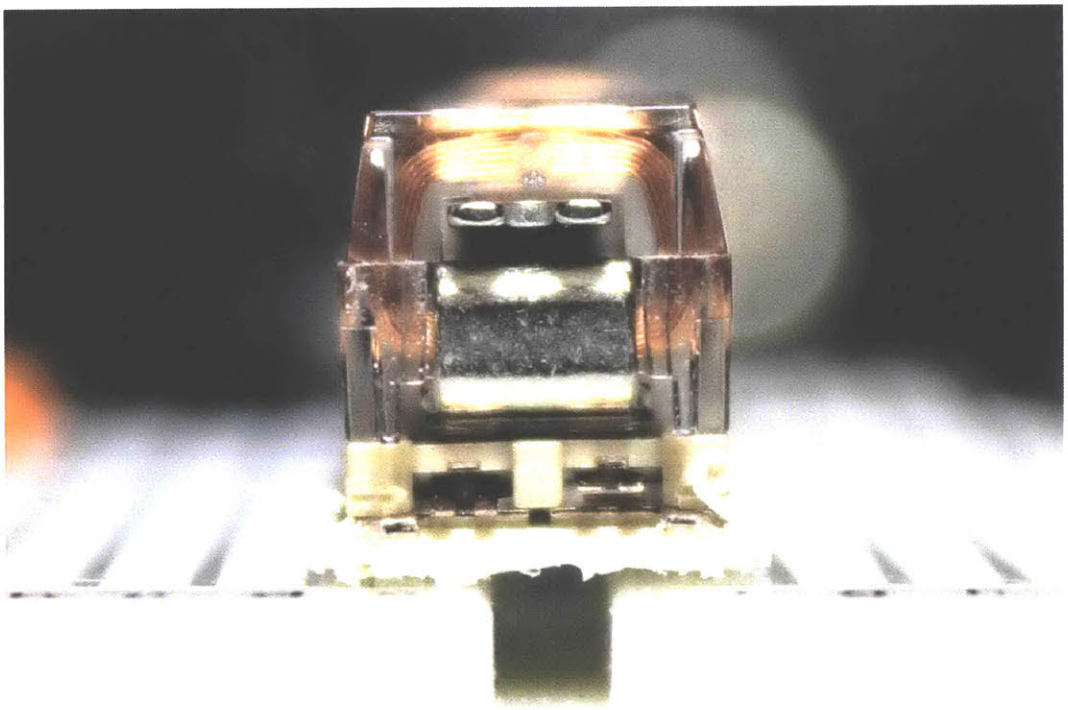

Figure 5-1. A photograph showing the relay damaged while testing the model-scale z-source circuit breaker.

This unexpected occurrence opened a new avenue of research and an opportunity to possibly make an innovative circuit design more suitable for operational employment.

[1]Ironically, this equipment failure illustrates why mechanical contacts are ill-suited for use in interrupting DC fault currents.

5.2 Faults for Which Protection Is Not Shown

For a mechanical circuit breaker the mechanism that opens the circuit breaker when a trip is commanded, normally strong springs, is inherently charged when the circuit breaker is closed[2]. An Eaton VCP-W Vacuum Circuit Breaker, representative of a naval MVAC circuit breaker, is shown in Figure 5-2 to illustrate this example. This image shows the circuit breaker in the shut condition with the closing springs (parts 1 and 11) relaxed and the opening spring (part 12) stretched and ready to force the contacts open. The analog to these springs in the crossed and series-connected z-source circuit breakers is the shunt capacitors. The difference between the springs and the capacitors, though, is that the thyristor can be fired without the capacitor being charged, but the typical mechanical circuit breaker generally cannot be closed if the opening springs are not stretched (or compressed, depending on the particulars of the circuit breaker).

Without the circuit-breaking energy stored somewhere in the mechanism the circuit breaker cannot interrupt the flow of current. In the z-source circuit breaker, the initially uncharged capacitors mean that the circuit breaker will have a brief period, on the order of about one to two millisecond in simulations, where it cannot be turned off. This characteristic introduces a new consideration for power system design: the circuit breaker will not be capable of interrupting current, nominal or rated fault, throughout its normal operating regime. Protection cannot be shown for a fault that occurs during the initial shunt capacitor charging transient or for closing the circuit breaker onto a short-circuited bus. Figures 5-3 and 5-4 show the circuit breaker's behavior during these faults. Current through the thyristor grows in the few milliseconds after fault initiation and reaches some steady-state value governed by the resistance in the thyristor, blocking diode, and fault. The shunt capacitor does not discharge to maintain voltage at the thyristor's cathode because it is still charging. In the simulation, this condition persists indefinitely. In a real power system this could lead to a fire or other damage as components overheat. Figure 5-5 shows what

[2]This assumes that there is no mechanical failure of the springs, which is a fair assumption if routine inspections and preventive maintenance are conducted on the circuit breaker.

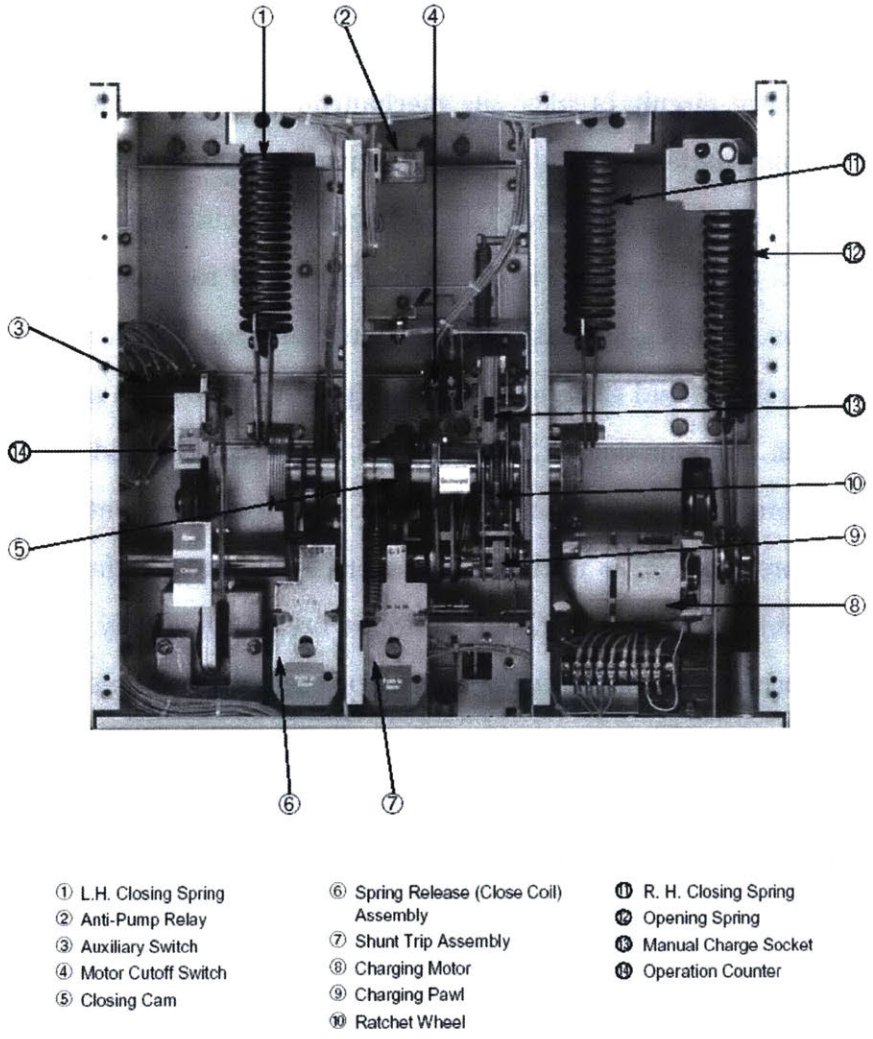

Figure 5-2. A picture of Eaton VCP-W Vacuum Circuit Breaker showing internal components, including opening springs. Source: Eaton, used with permission [15].

this fault looks like in the model-scale system. In this test the current was limited by the power supply to 2 A. Once that current limit was reached the output voltage drooped, which is why the traces in Figures 5-4 and 5-5 look so different.

This lack of protection is not because the inherent rise-in-current mechanism will not detect the condition; it is because the thyristor cannot be reverse biased, so neither manual trip mechanism will function. In these circumstances other means must be used to de-energize the faulted bus, such as opening an upstream circuit breaker or turning off a power converter and intentionally dropping additional loads, or by applying some external voltage across the thyristor using additional circuity.

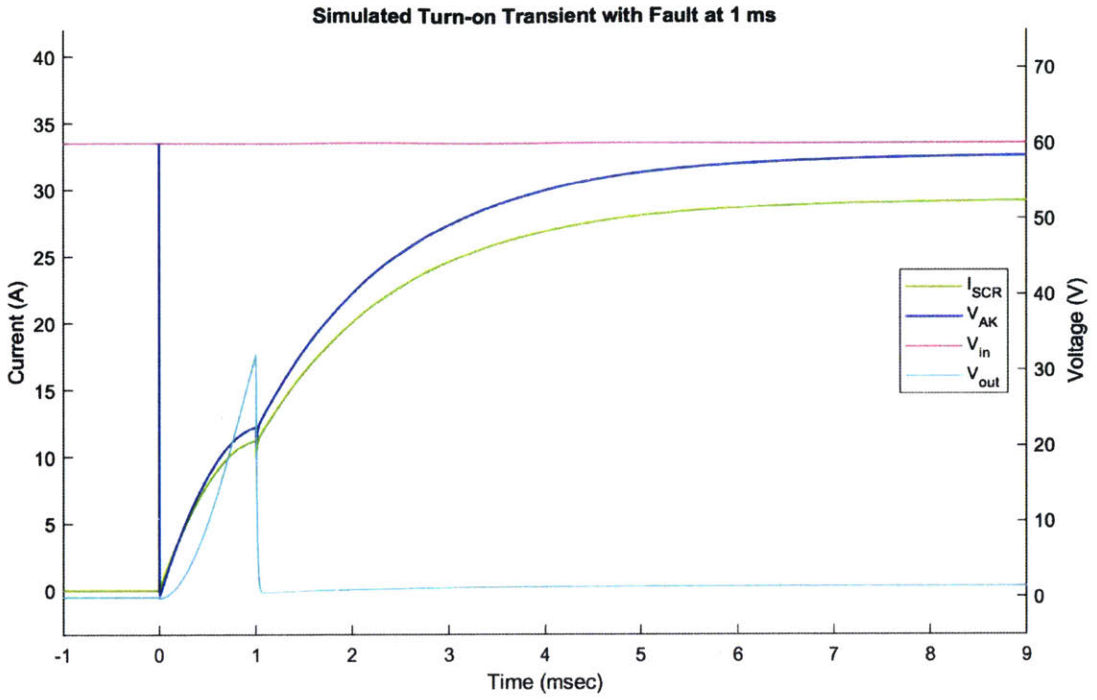

Figure 5-3. Simulated transients in a series-connected z-source circuit breaker for a fault initiated after the thyristor is gated on but before the system reaches steady-state operation.

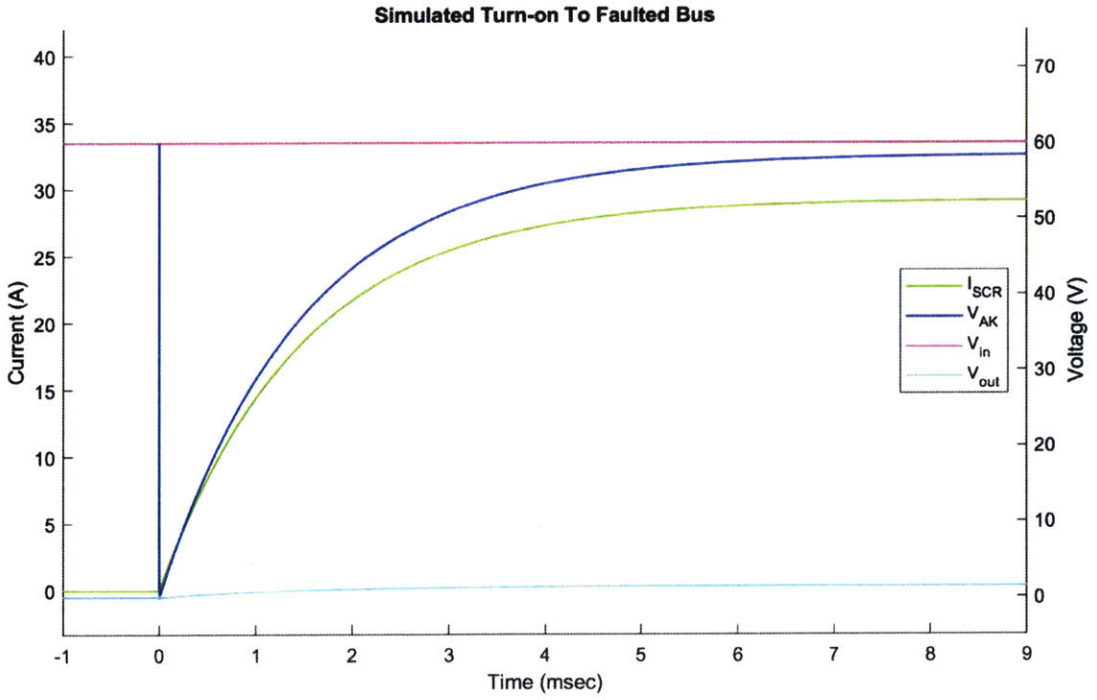

Figure 5-4. Simulated transients in a series-connected z-source circuit breaker for a fault initiated before the circuit breaker is closed.

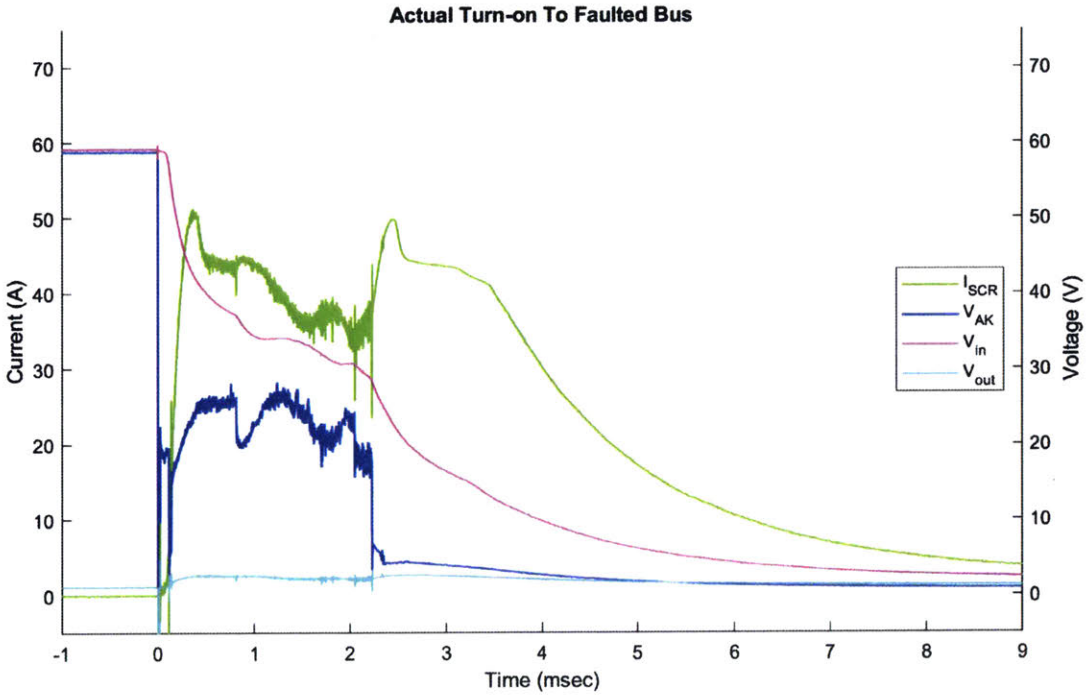

Figure 5-5. Actual transients in a series-connected z-source circuit breaker for a fault initiated before the circuit breaker is closed.

5.3 Possible Circuit Modifications

As in Chapter 3, the discussion here will focus on the series-connected z-source circuit breaker, but the concepts can be extended to the other topologies as well. The previous iterations of the series-connected z-source circuit breaker are limited by the need to have a charged shunt capacitor as a source of stored energy to open the circuit when tripped. This condition is met once the circuit breaker reaches steady-state operation. A method to charge the shunt capacitor before energizing the load bus is necessary to show adequate fault protection throughout all phases of operation. The z-source circuit breaker has the attractive quality that it can be implemented with a minimal number of components, all of which are passive or uncontrolled except the thyristor. To keep this advantage, any modifications should add only the bare minimum number of additional components. Ideally, none of these added components will result in additional power losses in the circuit breaker and will require minimum control input.

Any practical implementation of a circuit breaker will require a manual trip mechanism, so the implementations of the z-source circuit breaker shown in Figures 3-7 and 3-8 should serve as the starting point for modification. Examining the circuit in Figure 3-8, an element has to be placed in series with the output to block current flow and allow the shunt capacitor to initially charge. Any non-ideal component placed in this location will result in some power dissipation that is proportional to current drawn by the load. The circuit in Figure 3-7 already has a blocking diode that is in series with the output. If the blocking diode could be replaced with a different element, some sort of active switching device, there is an opportunity to modify this implementation of the circuit breaker without introducing new losses.

The blocking diode, D_3, in the circuit in Figure 3-7 can be replaced with a thyristor. This modification is shown in Figure 5-6 in blue. This substitution has no impact on normal circuit operations once the circuit breaker is turned on and has reached steady-state operation. The thyristor will block reverse current, as did the diode, when the circuit breaker is manually tripped. The power lost in the diode and the

thyristor should be similar in magnitude as well. This modification will require modified control signals. The circuit breaker now has two active switching devices, so two gating signals will be required for proper functionality.

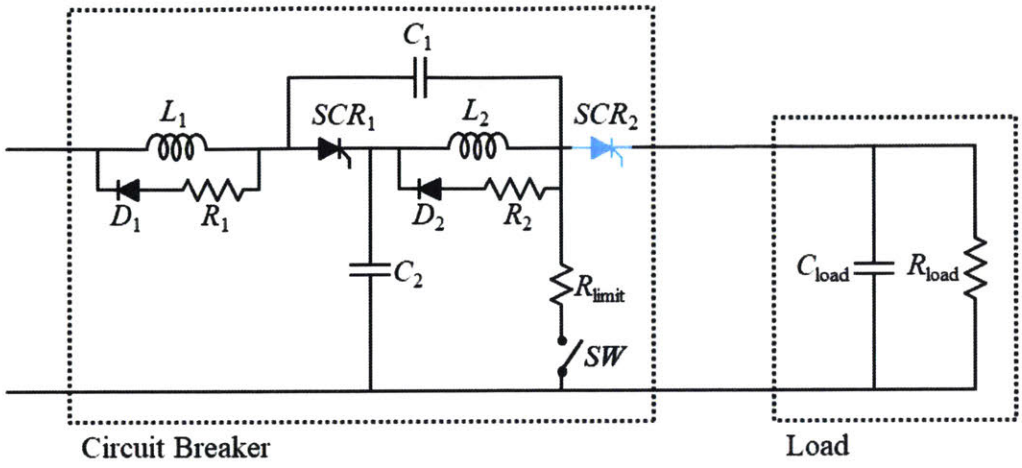

Figure 5-6. A modified series-connected z-source circuit breaker topology that pre-charges the shunt capacitor.

There are multiple ways to configure these gating signals but the one that seems most advantageous is a signal that turns on the primary thyristor, SCR_1, while capacitor C_2 charges and continues until SCR_2 is fired. The gating signal for SCR_2 can be a brief pulse to initiate current flow to the load and only needs to be applied long enough so that latching current can be achieved. This gating strategy is illustrated in Figure 5-7. Simulation in LTSpice was unable to confirm that this configuration provided additional protection during the initial transient and more work is required to understand if this is because of the recognized model inaccuracies during this phase of the circuit breaker operation or if there is some other shortcoming in the circuit.

Another gating scheme worth investigating is using the same gating signal simultaneously on both SCR_1 and SCR_2, also shown in Figure 5-7. This gating method offers the benefit that it preserves the control simplicity of the baseline topology. To take advantage of this gating scheme the components in the circuit breaker need to be adjusted. The circuit shown in Figure 5-6 allows C_2 to passively pre-charge. In

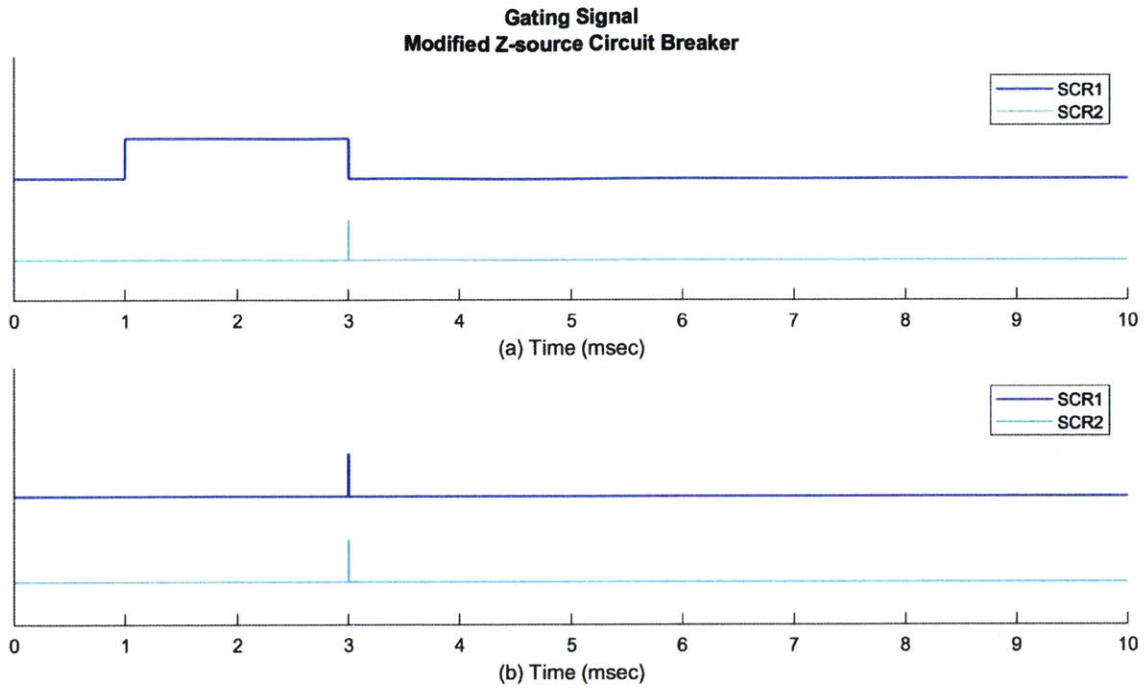

Figure 5-7. Gating signals used in the simulation model of the modified series-connected z-source circuit breaker.

the base topology C_1 is connected to through the load to ground and will charge to source voltage but C_2 remains uncharged. In the modified topology C_1 and C_2 form a voltage divider between the source and ground, where the voltage across C_2 can be found using

$$V_{C_2} = \frac{C_1}{C_1 + C_2} V_{source}$$

The level to which C_2 can pre-charge is determined by the ratio of C_1 to C_2. Using the parameters calculated in Appendices C and D the capacitors will charge to equal voltages. The minimum value for C_2 is a function of the $\frac{di}{dt}$ that will trip the breaker, so it is not feasible to alter its capacitance. Instead, the value of C_1 can be raised to a value that allows C_2 to pre-charge to near source voltage. As was the case with the other gating scheme, simulation in LTSpice was unable to confirm that this configuration provided additional protection during the initial transient and more work is required.

5.4 Alternative Integration Options

The likelihood of a fault occurring while the circuit breaker is turning on is small[3] compared to that of a fault occurring once the turn-on transient is over because it represents a miniscule amount of the total operating time. The consequences of such a fault are as severe as at any other time, though, so protection needs to be provided during the turn-on transient. Since the proper operation of a modified z-source circuit breaker could not be verified during this research, other ways to compensate for the protection gaps were considered. It has long been normal practice to provide multiple layers of fault protection and isolation in naval power systems, specifically in the form of selective tripping [12], [14]. In many current naval power systems the primary and secondary protective devices are often very similar, usually some variant of a mechanical circuit breaker. For the case of the z-source circuit breaker a second layer of protection can be provided by a different type of protective device that can interrupt fault currents during the periods when the z-source circuit breaker's capacitors are coming to equilibrium.

One such arrangement could feature multiple z-source circuit breakers that are all protected by one upstream circuit breaker, as shown in Figure 5-8. This circuit breaker needs to be a different type of circuit breaker, such as a large mechanical circuit breaker or hybrid mechanical circuit breaker [31]. A limited number of mechanical circuit breakers may be appropriate if used in this type of configuration because their numbers are limited so the total volume required by them is also limited. The circuit breaker could also be one of a number of types of solid-state devices, including an SCR flip-flop [32], an IGCT-based circuit breaker [33], or an IGBT-based circuit breaker [34]. The use of a larger or more complex device to provide this second layer of protection is offset by the reduced number required if the primary protection is provided by z-source circuit breakers.

Another viable arrangement, illustrated in Figure 5-9, is very similar but replaces the upstream circuit breaker with a power conversion module. Rather than opening

[3]The likelihood of closing a circuit breaker onto a faulted bus can be minimized by conducting some sort of ground impedance check prior to energizing the bus.

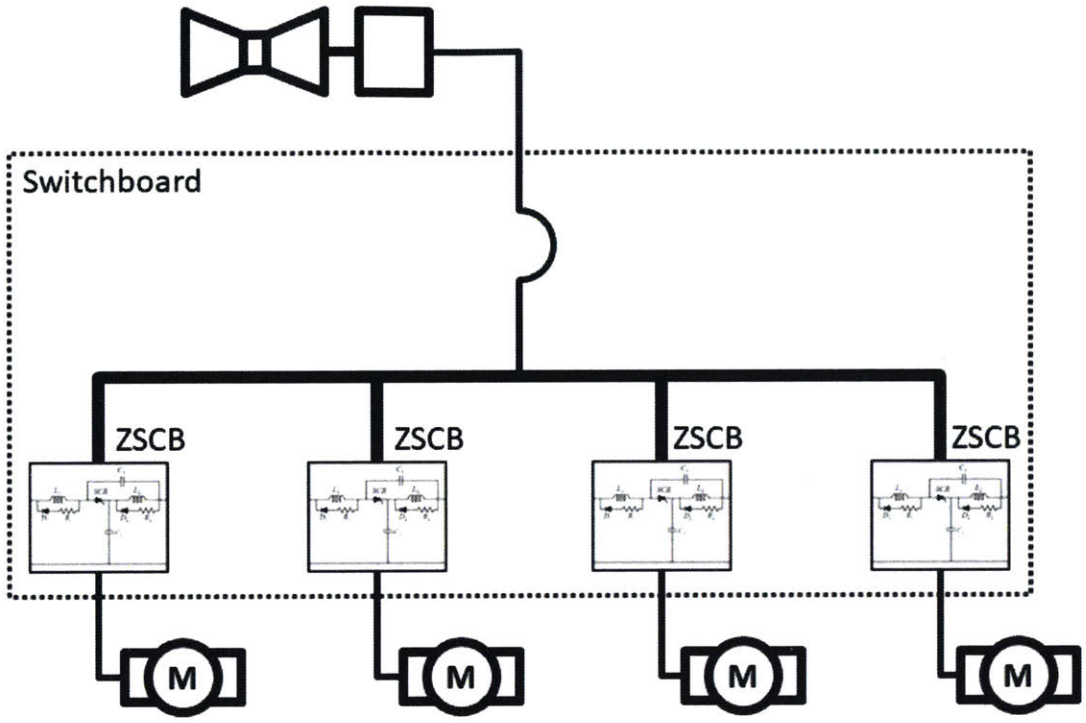

Figure 5-8. Arrangement in which one circuit breaker provides secondary protection to four circuits protected by z-source circuit breakers.

a circuit breaker as a protective action the power conversion module rapidly drives its output to zero as the protective action. This arrangement further leverages the strength of power electronics. If this arrangement is incorporated into one panel or switchgear cabinet then the control systems for the circuit breakers and power conversion modules can be integrated and allow for potentially faster fault identification and clearing. A combination power converter and circuit breaker has been proposed previously [35], although the topology used for the circuit breaker portion of that circuit is a different topology than those covered here. The converter is also constructed in such a way that the z-source circuit breaker also functions as an output filter to reduce the number of passive energy storage components required.

These arrangements allow z-source circuit breakers to be incorporated into a naval power system where their benefits, specifically very fast protective action that limits the magnitude of the fault current, can be leveraged while their shortcomings can be minimized. These arrangements facilitate incorporation without depending on adding

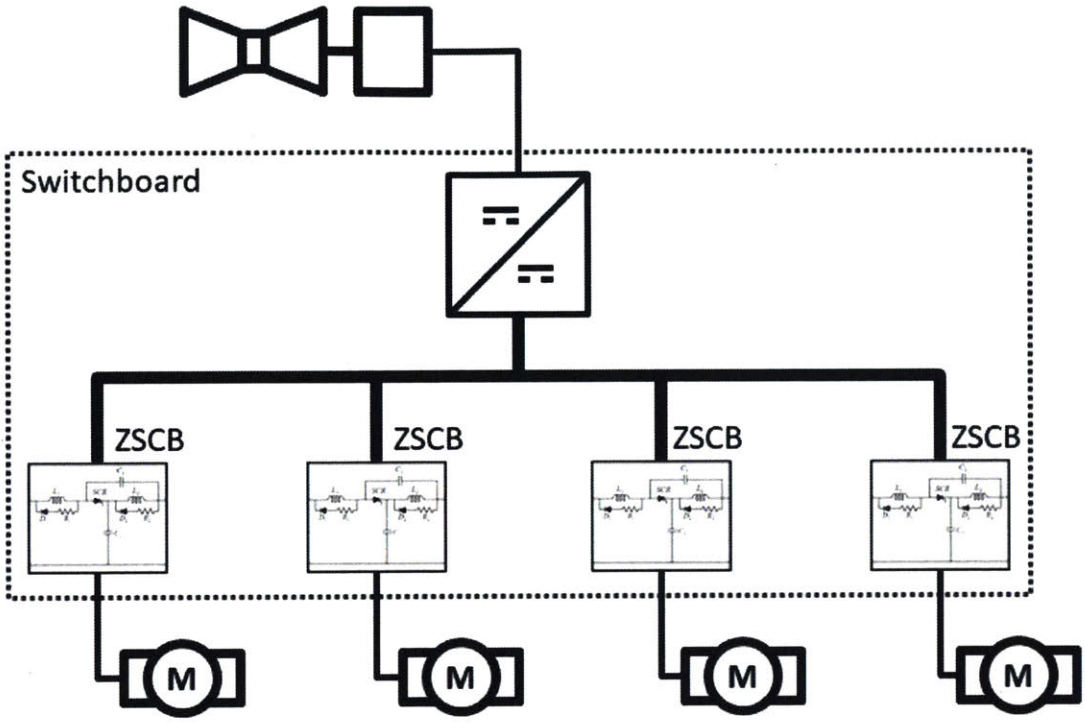

Figure 5-9. Arrangement in which one power conversion module provides secondary protection to four circuits protected by z-source circuit breakers.

further capabilities into the z-source circuit breaker as well.

Chapter 6

Conclusions and Recommendations for Further Study

6.1 Further Work

As is the case in many research endeavors, some questions were answered but new questions arose. The most important question that arose over the course of this project concerns the behavior of the z-source circuit breaker when a fault occurs during the circuit breaker's turn-on transient. This question was partially addressed in Chapter 5 but certainly merits more research. In support of this effort the LTSpice model developed during this project must be improved to more accurately model turn-on behavior. Additionally, the control scheme for turning the model-scale circuit breaker on and off must be modified for precise timing or coordination with fault insertion.

6.2 Conclusion

Detailed parameters for a representative naval MVDC power system were compiled to support modelling a "typical" system despite no such system exiting in full form. The results from Chapter 4 show that commercially available components are available for appropriately rated naval MVDC z-source circuit breakers and the discussion in

Chapter 5 shows how the devices can be incorporated into a deployable system. The z-source circuit breaker is a solution for some of the problems described in the NGIPS Development Roadmap, specifically that it can rapidly isolate faults while minimizing the magnitude of the peak fault current. The development of the z-source circuit breaker over the past nine years has advanced it to a point that it can be integrated with other existing technologies to provide multiple layers of protection to a given electrical load or zone of protection in much the same way that naval engineers and power system engineers have become accustomed to doing over the 130+ years of naval electrification.

Appendix A

List of Acronyms

AC	Alternating Current
AC	Collier (Navy ship type)
AWG	American Wire Gauge
CV	Aircraft Carrier
DC	Direct Current
DDG	Guided Missile Destroyer
HFAC	High Frequency Alternating Current
IEEE	Institute of Electrical and Electronics Engineers
IGBT	Insulated-Gate Bipolar Transistor
IGCT	Integrated Gate-Commutated Thyristor
IPNC	Integrated Power Node Center
IPS	Integrated Power System
MVAC	Medium Voltage Alternating Current
MVDC	Medium Voltage Direct Current
NAVSEA	Naval Sea Systems Command
NGIPS	Next Generation Integrated Power Systems
PCM	Power Conversion Module
SCR	Silicon Controlled Relay
SPICE	Simulation Program with Integrated Circuit Emphasis
SS	Single-screw Steamship

T-AKE	Dry Cargo/Ammunition Ship
USCGC	United States Coast Guard Cutter
USS	United States Ship
WAGB	Icebreaker, Coast Guard

Appendix B

LTSpice Simulation Models

The circuits in this project were simulated in LTSPICE XVII. Thyristor models are not included in LTSpice, so the functionality of this elements was achieved using a subcircuit composed of more basic element. This subcircuit model, developed with the assistance of Alex Hansen, is illustrated in Figure B-1. The model could be made more accurate in some aspects by connecting the net attached to the negative sensing terminal of $S1$ to the cathode net K. This connection gives more accurate behavior for turn-on behavior because it becomes governed by V_{GK} rather than by V_{G-gnd}. This quality is especially important when the thyristor is used in an AC circuit. This connection causes unintended issues in a DC circuit, such as the z-source circuit breaker, that leads to inaccurate simulations. The charge stored in $C1$ leaks out over the course of milliseconds due to LTSpice requiring non-idealities in components like the switches, i.e. $R_{off} \neq 0$, and causes the thyristor to turn off when it should remain on. Severing this connection and connecting the negative sensing terminal of $S1$ to ground solve the charge leakage problem but turn-on behavior becomes governed by V_{G-gnd} instead of V_{GK}. In the z-source circuit breaker models discussed later in this appendix this is not a problem because the gating signals are only applied in states when $V_{GK} \approx V_{G-gnd}$. As long as this limitation is respected the thyristor model presented here is adequate for these circuits.

The block of components that makes up the thyristor subcircuit was included in both models used for this project directly in the model rather than as a separate

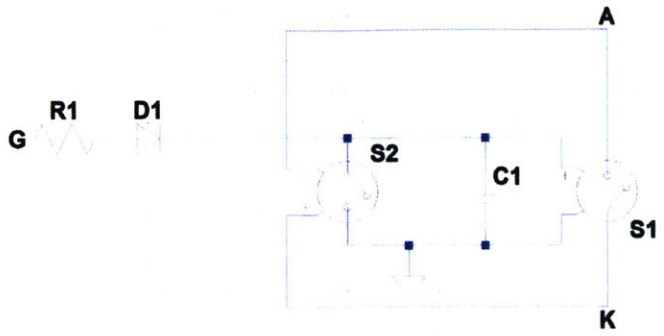

Figure B-1. LTSpice circuit model of a thyristor.

subcircuit file to allow examination of the inner workings of the device and confirm the thyristor model behaved as expected. The series-connected z-source circuit breaker model used for Chapters 3 and 5 is shown in Figure B-2. The modified series-connected z-source circuit breaker model used for Chapter 5 is shown in Figure B-3. The SPICE netlists for each model are also given in this appendix following each model diagrams.

B.1 Series-connected Z-source Circuit Breaker

This model was verified against the scale model described in Appendix D. There are some inaccuracies in the turn-on transients that are a result of idealizations in the thyristor simulation model and the assumption that load resistance is constant. In the scale model the load resistance increases as the filament of the light bulb warms. The model accurately reflects circuit operation once the load has reached steady-state operating conditions. The 10 nanosecond maximum time step, along with use of the alternate solver, were necessary to achieve proper model functionality. Longer time steps resulted in no protective action when a fault was inserted. Use of the normal solver produced inconsistent results and resulted in excessive simulation times.

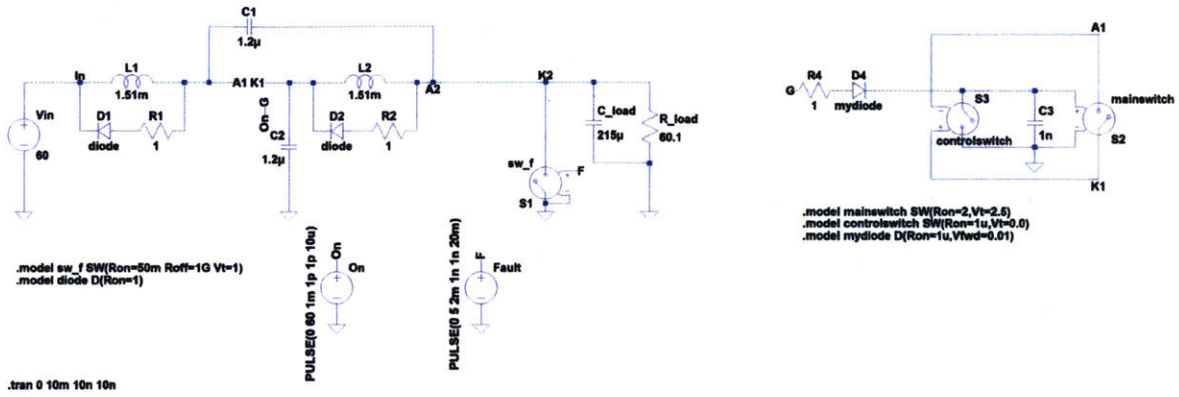

Figure B-2. LTSpice circuit model of the series-connected z-source circuit breaker.

```
*Series-connected z-source circuit breaker
Vin In 0 60 Rser=0
L1 In A1 1.51m
L2 K1 K2 1.51m
C1 K2 A1 1.2µ
C2 0 K1 1.2µ
D1 N003 In diode
D2 N004 K1 diode
C_load K2 0 215µ
R1 A1 N003 1
R2 K2 N004 1
R_load K2 0 60.1
S1 0 K2 F 0 sw_f
V§On G 0 PULSE(0 60 1m 1p 1p 10u)
V§Fault F 0 PULSE(0 5 2m 1n 1n 20m)
S2 K1 A1 N002 0 mainswitch
S3 N002 0 K1 A1 controlswitch
C3 N002 0 1n Rpar=0
D4 N001 N002 mydiode
R4 G N001 1
.model D D
```

```
.model sw_f SW(Ron=50m Roff=1G Vt=1)
.model diode D(Ron=1)
.model controlswitch SW(Ron=1u,Vt=0.0)
.model mydiode D(Ron=1u,Vfwd=0.01)
.model mainswitch SW(Ron=2,Vt=2.5)
.tran 0 10m 10n 10n
.backanno
.end
```

B.2 Modified Series-connected Z-source Circuit Breaker

This model was developed from the model in the previous section to test ideas for possible circuit design improvements. A scale model was not available for comparison of this simulation model. This model likely suffers from the same inaccuracies during turn-on as the previous simulation model. As in the first model a 10 nanosecond maximum time step was enforced and the alternate solver was used.

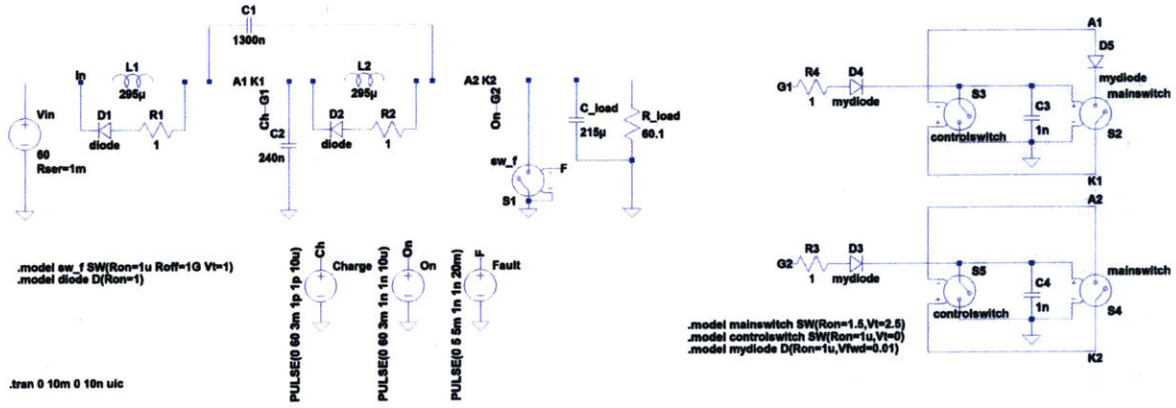

Figure B-3. LTSpice circuit model of the modified series-connected z-source circuit breaker from Chapter 5.

```
*Modified series-connected z-source circuit breaker
Vin In 0 60 Rser=1m
L1 In A1 295µ
L2 K1 A2 295µ
```

```
C1 A2 A1 1300n
C2 0 K1 240n
D1 N004 In diode
D2 N005 K1 diode
C_load K2 0 215µ Rser=500m
R1 A1 N004 1
R2 A2 N005 1
R_load K2 0 60.1
S1 0 K2 F 0 sw_f
V§Charge G1 0 PULSE(0 60 3m 1p 1p 10u)
V§On G2 0 PULSE(0 60 3m 1n 1n 10u)
V§Fault F 0 PULSE(0 5 5m 1n 1n 20m)
S2 K1 N003 N002 0 mainswitch
S3 N002 0 K1 A1 controlswitch
C3 N002 0 1n Rpar=0
D4 N001 N002 mydiode
R4 G1 N001 1
S4 K2 A2 N007 0 mainswitch
S5 N007 0 K2 A2 controlswitch
C4 N007 0 1n Rpar=0
D3 N006 N007 mydiode
R3 G2 N006 1
D5 A1 N003 mydiode
.model D D
.model sw_f SW(Ron=1u Roff=1G Vt=1)
.model diode D(Ron=1)
.model controlswitch SW(Ron=1u,Vt=0)
.model mydiode D(Ron=1u,Vfwd=0.01)
.model mainswitch SW(Ron=1.5,Vt=2.5)
.tran 0 10m 0 10n uic
```

```
.backanno
.end
```

Appendix C

Calculation of Model Parameters

The parameters used in the scale model are based on the notional system values laid out in NGIPS Technology Development Roadmap [10] and Design Considerations for a Reference MVDC Power System [36]. The parameters are summarized in Table C.1.

Table C.1. Summary of full-scale and model parameters.

Parameter	Full-scale System	Model System
V_{source}	6000 V	60.0 V
I_{load}	166.7 A	0.985 A
R_{load}	36.0 Ω	60.9 Ω
P_{load}	1 MW	59.1 W
C_{load}	364 µF	215 µF
$\|Z_{0,line}\|$	29.6 Ω	50.0 Ω
G_{fault}	50.0 S	29.6 S
L_{min}	N/A	295 µH
C_{min}	N/A	239 nF

C.1 Full-scale System

C.1.1 Source Voltage (V_{source})

The distribution voltage levels currently under consideration are 6 kV, 12 kV, and 18 kV[30]. NAVSEA has focused recent ship studies on vessels employing 6 kV

distribution systems rather than examining higher voltages[37]. The full-scale source voltage for this notional system, $V_{source,\ f}$, will be set to 6 kV.

C.1.2 Load Power (P_{load})

Based on the information presented in [36], the power consumed by a notional load could range from 500 kW to 10 MW. For this model, the load will be based on that a single IPNC, which drives the capacity of an output module in a PCM-1A. The full-scale load power, $P_{load,\ f}$, will be set at 1 MW. This allows determination of the full-scale load current, $I_{load,\ f}$:

$$P = IV \longrightarrow I_{load,\ f} = \frac{P_{load,\ f}}{V_{source,\ f}} = \frac{1\ MW}{6\ kV} = 166.7\ A$$

This assumes that the voltage drop across the z-source circuit breaker is negligible, so that $V_{load} \approx V_{source}$.

C.1.3 Load Resistance (R_{load})

For the full-scale model the load resistance, $R_{load,\ f}$, can be computed using Ohm's law and the values determined earlier:

$$V = IR \longrightarrow R_{load,\ f} = \frac{V_{load,\ f}}{I_{load,\ f}} = \frac{6000\ V}{166.7\ A} = 36.0\ \Omega$$

C.1.4 Load Capacitance (C_{load})

The full-scale estimate for C_{load} comes from an examination of the a Modular Multilevel Converter in Florida State University's Center for Advanced Power Systems discussed in [18]. Impedance data for the converter was collected over a range of frequencies. The imaginary component of this impedance $Z_{load} = R_{load} + jX_{load}$ represents the converter's capacitance, which can be calculated using

$$X_{load} = X_C = \frac{1}{\omega C_{load}} \longrightarrow C_{load} = \omega X_C$$

The capacitance was estimated at three frequencies, shown in Table C.2. These values were averaged to arrive at

$$C_{load} = 363.6\ \mu F$$

Table C.2. Modular Multilevel Converter capacitance.

Frequency	X_C	C_{load}
1 Hz	434.7 Ω	366.2 µF
10 Hz	44.56 Ω	357.2 µF
50 Hz	8.660 Ω	367.6 µF

C.1.5 Line Characteristic Impedance (Z_0)

Representative cable characteristics for naval MVDC cable in typical installation configurations are [28]:

$$R_{line,\ f} = 47.0\frac{\mu\Omega}{m}$$
$$C_{line,\ f} = 561\frac{pF}{m}$$
$$L_{line,\ f} = 490\frac{nH}{m}$$

Leakage current in transmission and distribution lines is generally very small compared to the transmitted current so conductance, $G_{line,\ f}$, is approximately zero. The characteristic line impedance can be calculated using:

$$Z_0 = \sqrt{\frac{R + j\omega L}{G + j\omega C}}$$

At first glance the frequency for the system might appear to be zero because it is a DC system. The load in the system is a PCM-1A, a type of switching regulator. The system examined by Chauncey had an effective switching frequency of 2 kHz[18], which will be the system frequency used here. The scaling factor for time units in

this model is unity, so $\omega_f = \omega_m$. The full-scale characteristic impedance is:

$$\bar{Z}_{0,\,f} = \sqrt{\frac{(47.0\ \mu\Omega) + j(4000\pi\ rad/sec)(490\ nH)}{j(4000\pi\ rad/sec)(561\ pF)}} = 29.6 - j0.113\ \Omega$$

$$|\bar{Z}_{0,\,f}| = 29.6\ \Omega$$

C.1.6 Fault Properties

The fault examined in this model will be a short circuit. The full-scale fault considered in this study is the same fault from Corzine's and Ashton's work, a maximum conductance, $G_{fault,\,f}$, of 50 S[13].

C.2 Per-unit Normalization

The model system will be scaled to maintain the same per-unit and time characteristics as the full-scale system. For this system it is convenient to set the base quantities shown in Table C.3 using $V_{base} = V_{source}$ and $Z_{base} = |\bar{Z}_{0,\,f}|$.

Table C.3. System base quantities.

Parameter	Full-scale System	Model System
V_{base}	6000 V	60.0 V
I_{base}	202.7 A	1.20 A
Z_{base}	29.6 Ω	50.0 Ω
P_{base}	1,000,000 W	72 W

Using the established base quantities for the full-scale system and assuming a 50 m load-side cable length, the per-unit quantities shown in Table C.4 can be calculated.

Table C.4. Per-unit normalization of system characteristics.

Parameter	Per-unit Value
V_{source}	1.000
I_{load}	0.821
R_{load}	1.218
R_{line}	7.951×10^{-5}
P_{load}	0.821
G_{fault}	1478

C.3 Model-scale System

C.3.1 Source Voltage (V_{source})

The source voltage for the scale model is limited by the laboratory facilities and electrical safety consideration. The model-scale source voltage, $V_{source,\ m}$, will be set to 60 V.

C.3.2 Line Characteristic Impedance (Z_0)

The line characteristic impedance for the model will be set at 50 Ω due to availability of materials for the model system.

C.3.3 Load Characteristics

Load Current (I_{load}) and Resistance (R_{load})

The model-scale load current is scaled on a per-unit basis:

$$I_{load,\ m} = i_{load} \times I_{base,\ m} = (0.821\ p.u.)(1.200\ A) = 0.985\ A$$

The model-scale load resistance is also scaled in this way:

$$R_{load,\ m} = r_{load} \times Z_{base,\ m} = (1.218)(50.0\ \Omega) = 60.9\ \Omega$$

Load Capacitance (C_{load})

Scaling for the reactive components in the system is accomplished to maintain the the full-scale and model-scale time characteristics equal. For capacitive and inductive elements this means that the the full-scale and model-scale time constants are equal:

$$\tau_f = \tau_m$$

Capacitive element values can be calculated using

$$R_f C_f = R_m C_m \longrightarrow C_m = \frac{R_f C_f}{R_m}$$

$$C_{load,\ m} = \frac{(36.0\ \Omega)(364\ \mu F)}{60.9\ \Omega} = 215\ \mu F$$

C.3.4 Z-source Circuit Breaker Passive Components

The capacitors and inductors contained within the z-source circuit breaker are used to set the maximum allowable value time rate of current change, $\frac{dI}{dt}$. These values cannot be set in isolation because the current rise also depends on the reactive elements in the rest of the system. These values are not scaled directly from the full-scale system but are instead calculated directly from the model-scale system values.

Capacitors

The minimum capacitance required for proper operation can be calculated using the equations developed by Corzine and Ashton [13]:

$$C_{min} = \frac{2C_{load} I_{scr}}{V_{source} G_{fault} - I_{scr}}$$

In steady-state operation the current through the thyristor, I_{scr}, is equal to I_{load} by KCL. The fault condition must be scaled according to the same rules as resistances to find the model-scale fault conductance, $G_{fault,\ m}$:

$$G_{fault,\ m} = \frac{1}{R_{fault,\ m}} = \frac{1}{r_{fault} \times Z_{base,\ m}} = \frac{g_{fault}}{Z_{base,\ m}}$$

$$G_{fault,\ m} = \frac{1478\ p.u.}{50.0\ \Omega} = 29.6\ S$$

Given this information, the minimum capacitance required in the scale model z-source circuit breaker is

$$C_{min,\ m} = \frac{2(215\ \mu F)(0.985\ A)}{(60.0\ V)(29.6\ S) - (0.985\ A)} = 239\ nF$$

Inductors

The minimum inductance required for proper operation can be calculated using the equations developed by Chang, et al. [21]:

$$L_{min} = \frac{1}{3} R_{load}^2 C_{min}$$

Given the values calculated previously, the minimum inductance require in the scale model z-source circuit breaker is

$$L_{min,\ m} = \left(\frac{1}{3}\right)(60.9\ \Omega)^2(239\ nF) = 295\ \mu H$$

THIS PAGE INTENTIONALLY LEFT BLANK

Appendix D

Model Circuit Design

The circuit breaker considered in this experiment is the series-connected z-source circuit breaker proposed by Chang et al.[21]. The circuit breaker topology is shown in Figure 3-2, and repeated in this section as Figure D-1.

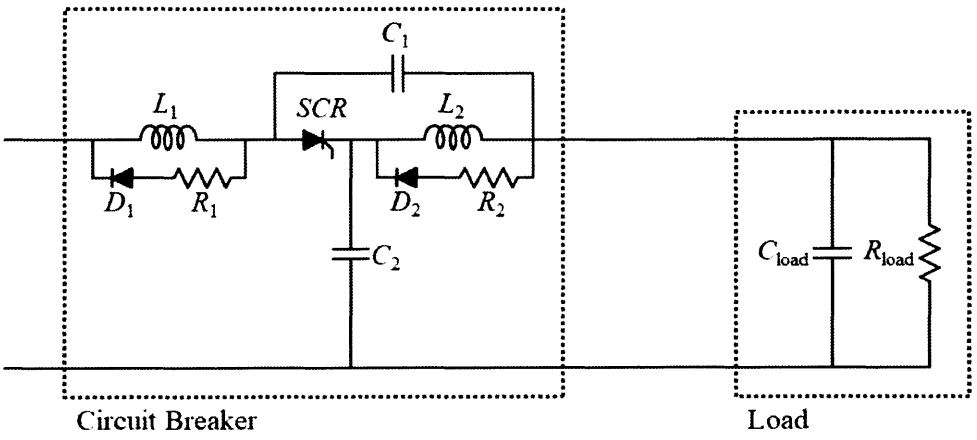

Figure D-1. Series-connected z-source circuit breaker topology.

D.1 Circuit Breaker Component Selection

D.1.1 Thyristor

The central component of the z-source circuit breaker is the thyristor, labeled "SCR" in Figure D-1. This was the first component selected and drove the other component selection decisions. The primary considerations for selecting this component are the voltage and current ratings. A secondary consideration for a suitable device is the latching current, which must be low enough that the predicted load current will keep the thyristor in the on state. The main thyristor is a VS-30TPS16 manufactured by Vishay Intertechnology and sourced from Digi-Key. The key characteristics of the device are summarized in Table D.1.

Table D.1. VS-30TPS16 key characteristics.

Parameter	Value
Peak off-state voltage ($V_{peak,\ off}$)	1600 V
Maximum RMS on-state current (I_{RMS})	30 A
Maximum latching current, (I_L)	200 mA
Typical turn-off time, (t_q)	110 µs

The current through the model-scale load, $I_{load,\ m}$, is sufficiently greater than I_L so the thyristor should remain on during steady-state operation without constantly apply a gating signal. Additionally, $I_{load,\ m}$ is sufficiently less than I_{RMS} that the expected currents will not damage the thyristor during testing. The maximum voltage will drive the voltage ratings of other components.

D.1.2 Capacitors

The selection of capacitors is relatively simple as it depends only on the expected voltage which will be applied to them. The maximum voltage that the system will be designed to sustain is the maximum voltage rating of the thyristor, 1600 V. Based on part availability, the capacitors for this circuit will each be comprised of two 120 nF EPCOS B32656T2124K000 capacitors arranged in parallel, for an equivalent

capacitance of 240 nF, slightly more than the minimum required value of 239 nF calculated previously. A pair of pads will be included on the circuit board design with each capacitor to allow fine-tuning the capacitance value as necessary.

D.1.3 Inductors

The inductors for this circuit must be selected to carry the anticipated maximum fault-induced current. As inductor current cannot change instantaneously, this current will be somewhere between the steady-sate load current and the fault current. This current can be calculated using equations developed in [21]:

$$i_L = I_{load} + \frac{V_{source}}{6L} \times \frac{K \times t^3}{C + 2C_{load}}$$

where C and L are at least the values calculated previously as C_{min} and L_{min} and K is the fault ramp rate:

$$K = \frac{G_{fault}}{\Delta t_{fault}}$$

Both Corzine [13] and Chang [21] consider faults ramping over 0.1 ms, which is a conservative value to use for this experiment. If the ramp time is longer then the magnitude of the K and i_L decrease.

$$K = \frac{29.6\ S}{0.1\ ms} = 9534\ \frac{S}{sec}$$

The maximum current through the inductor occurs at time

$$t = \sqrt{\frac{C + 2C_{load}}{2K}} = \sqrt{\frac{(239\ nF) + (2)(215\ \mu F)}{(2)\left(9534\ \frac{S}{sec}\right)}} = 1.06\ ms$$

and has a value of

$$i_{L,\ max} = (0.985\ A) + \frac{60.0\ V}{(6)(295\ \mu H)} \times \frac{\left(9534\ \frac{S}{sec}\right)(1.06\ ms)^3}{(239\ nF) + (2)(215\ \mu F)} = 1.88\ A$$

This fault-induced current is approximately twice the steady-state current.

Due to the limited selection of commercially-available appropriated inductors, custom inductors will be fabricated for this experiment.

D.1.4 Flyback Diodes

The flyback diodes in this circuit must withstand the maximum expected current and reverse voltage conditions. The maximum current which they be required to conduct is the maximum inductor current, assuming the load was instantaneously disconnected. This current, $i_{L,\ max}$ was previously calculated as 1.88 A. The maximum voltage rating for any component in this circuit will be 1600 V based on the rating of the thyristor. The Vishay Semiconductors VS-8EWS16SLHM3 will be used based on these criteria.

D.1.5 Damping Resistors

The constraint on the damping resistors is power dissipation. The maximum expected current is $i_{L,\ max}$. With current fixed, resistance value or power dissipation capacity can be selected and the third variable can be computed. Power resistors are readily available in 5 W packages, so the power will be set to that and maximum resistance calculated:

$$P = I^2R \longrightarrow R = \frac{P}{I^2} = \frac{5\ W}{(1.88\ A)^2} = 1.41\ \Omega$$

Power resistors are readily available in 1 Ωresistance, which meets the requirements laid out[1], so the damping resistors will be set to that value.

[1]The power resistors under consideration are rated for sort-time (5 second) overload to five times the nominal power rating.

D.2 Load Selection

The load is composed of two parts: the resistive component and the reactive component. For this system the reactive component is capacitive in nature.

D.2.1 Resistive Component

The resistance of the resistive component was calculated in Appendix C to be 60.9 Ω. This could be provided by using one adjustable power resistor but in this model it is achieved using an incandescent light bulb in parallel with an adjustable power resistor. Inclusion of the light bulb in the circuit provides a convenient visual indicator that the load bus has been de-energized. Incandescent light bulb filaments have a resistance that is highly dependent on temperature [38]. This means that the resistance of the variable resistor had to be set based on the hot resistance of the 40 W incandescent light bulb. It also means that circuit breaker tests should be conducted once the light has warmed to operating temperature.

D.2.2 Reactive Component

The capacitive component of the load is composed of capacitors arranged in a parallel to achieve the required total capacitance, 215 μF. This compound capacitive element is connected in parallel with the light bulb and the power resistor. Figure D-2 show a schematic representation of the load and Figure D-3 shows the load as built. The capacitors discussed in this section are housed in the junction box under the light bulb holder.

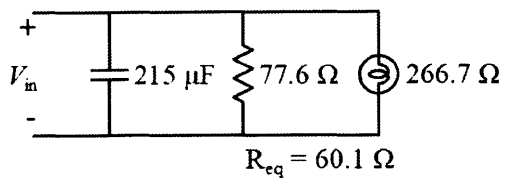

Figure D-2. A schematic of the load connected to the model-scale system.

Figure D-3. A photograph of the load connected to the model-scale system.

D.3 Fault

Two different fault insertion devices were built for the model system and are shown in Figure D-4. The first was a simple switch used to short-circuit the load bus. This was constructed as a light switch mounted in 1-gang electrical box. The switch was connected into the circuit using BNC connectors. This device was useful for initial testing of the model-scale system and confirming that the circuit breaker did indeed interrupt current flow, but it was not suitable for taking detailed, precisely-timed measurements for the analysis of Chapter 4. The second fault insertion device is a relay that short-circuits the load bus. The relay is controlled by a microprocessor, an Atmel ATtiny85, that opens and closes the relay based on the position of a light

switch. At its heart, the second device operates the same way as the first, but it also provides a signal to an oscilloscope to indicate the exact time that the fault is initiated. The oscilloscope triggering functionality was ultimately redundant once the circuit worked properly, as the oscilloscope was set to trigger on rising or falling V_{AK}.

The relay initially used in the second device was an Axicom V23105-A5001-A201. This relay has a manufacturer's rating of 220 VDC/3 A, though the safe operating region specified does not allow operation at maximum current and maximum voltage. The datasheet also lists a lower UL contact rating of 60 VDC/0.3 A. Even though the expected fault current will exceed the relay's ratings in either condition, this should be an acceptable component because it will only be used to make the fault circuit, it will not be used to break the circuit. The relay will only be opened one the load bus has been de-energized, either through circuit breaker action or manually turning off the power supply.

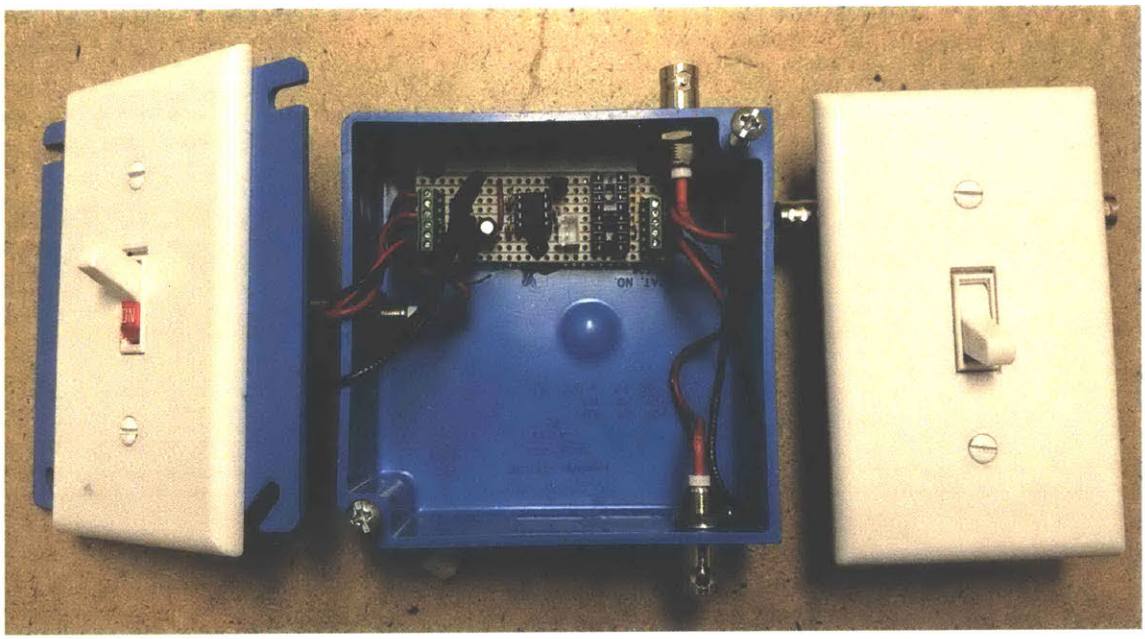

Figure D-4. A photograph showing the two fault insertion devices used for testing.

D.4 Power Supply

The model-scale system requires a DC power supply. It must be capable of providing 60 V and at least 2 A. Multiple power supplies readily available in the lab meet these requirements.

D.5 Circuit Board

The two-layer circuit board for the model-scale system was laid out using Autodesk EAGLE and was manufactured by OSH Park. Figure D-5 shows the schematic of the circuit breaker, Figure D-6 shows the circuit board's layout, and Tables D.2 lists the components used. Figure D-7 shows the assembled circuit breaker. A series of secondary boards were assembled to serve as various configurations of off switches as proposed by Chang et al.

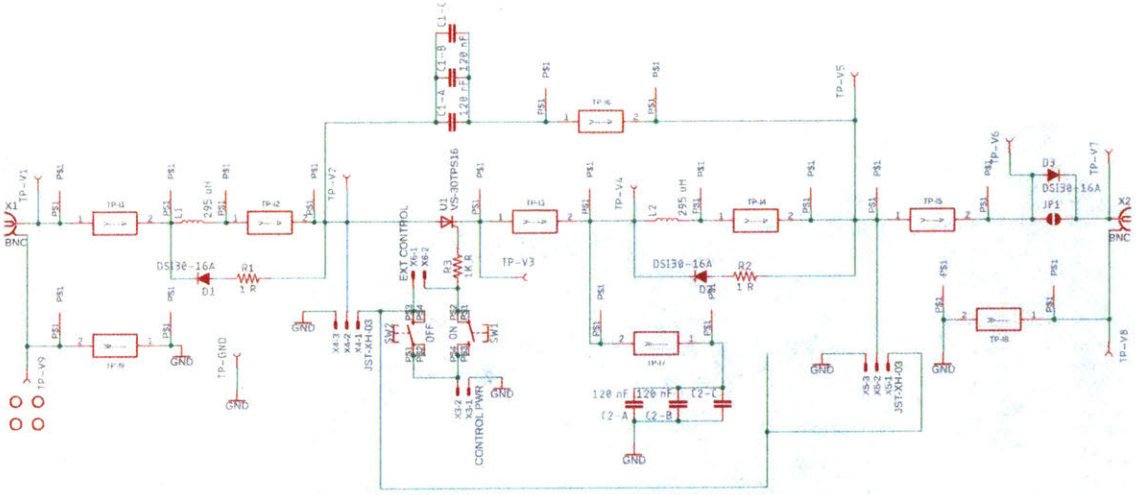

Figure D-5. Z-source circuit breaker schematic.

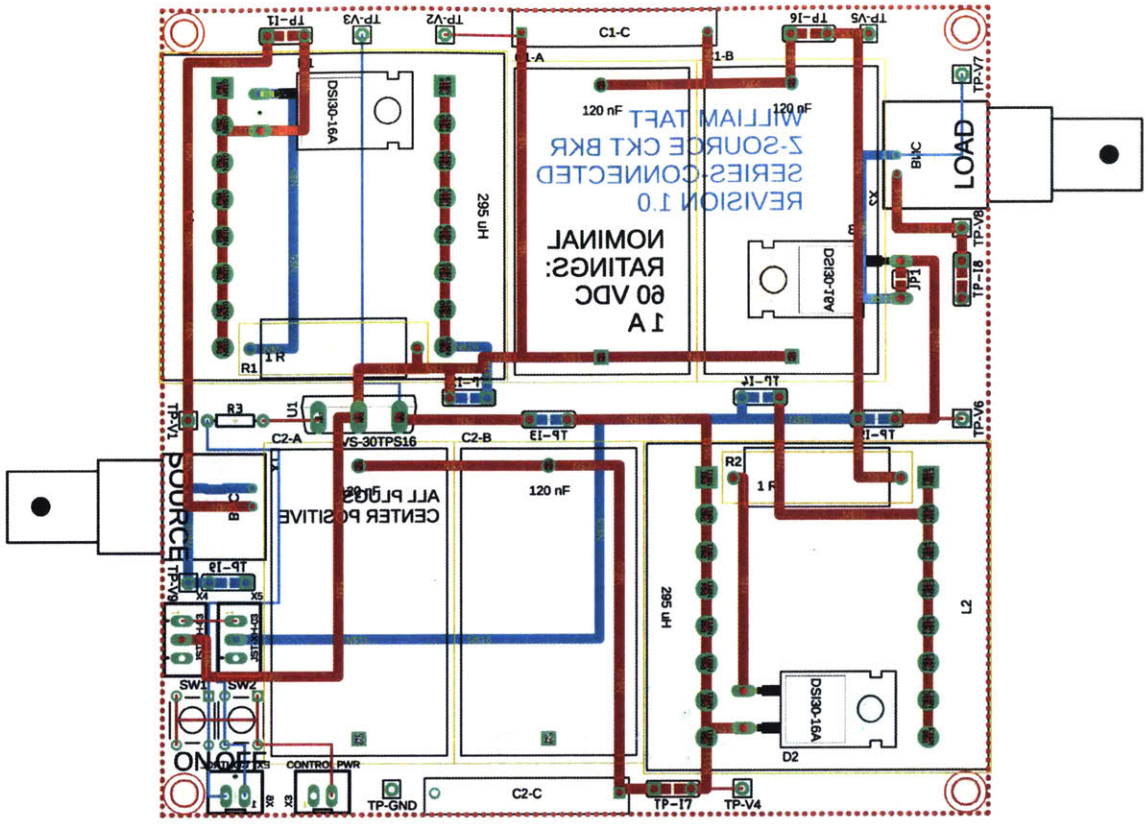

Figure D-6. Z-source circuit breaker layout showing both top and bottom (with reverse printing) layers.

Table D.2. Listing of main board circuit components for the initial design.

Component	Value	Part Number
U1 (Thyristor)	N/A	Vishay VS-30TPS16
L1/L2	295 µH (31 turns)	EPCOS AG B66364B1016T001 EPCOS AG B66363G0000X127 EPCOS AG B66364A2000X000
C1-A/C1-B/C2-A/C2-B	0.12 µF	EPCOS AG B32656T2124K000
R1/R2 (Damping resistor)	1 Ω/5 W	Ohmite WNE1R0FET
R3 (Current limiting resistor)	100 textOmega	N/A
D1/D2 (Flyback diode)	N/A	IXYS DSI30-16A
D3 (Blocking diode, optional)	N/A	IXYS DSI30-16A
SW1/SW2	Off-Mom	NKK Switches HP0215AFKP2-S
X1/X2	N/A	Molex 0731375003
X3/X4	N/A	JST B3B-XH-A
X5/X6 (Optional)	N/A	JST B2B-XH-A

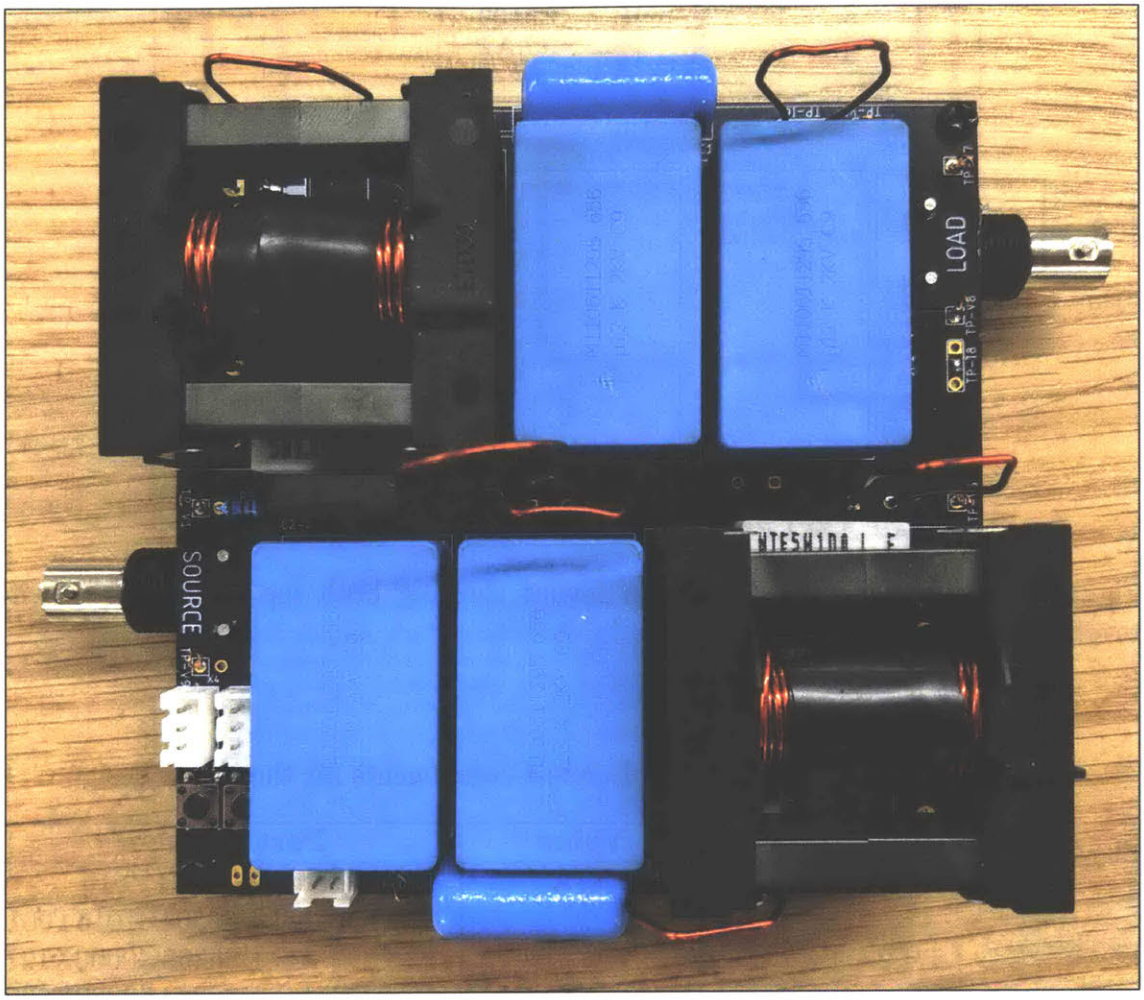

Figure D-7. The first assembled model-scale z-source circuit breaker with components rated for 1600 VDC.

D.6 Circuit Redesign

Testing did not initial go as planned. The circuit designed in the previous sections failed to properly interrupt the fault current and had to be reevaluated and redesigned. Fortunately, the printed circuit board did not have to be changed, only the components used to populate it.

The relay has a resistance of 20 mΩ when closed, giving a fault conductance of 50 S. This is greater than the required fault conductance of 29.6 S derived in Appendix C, so it should be a sufficient value to cause the circuit breaker to trip. However, experimental testing showed that this was not the case. Other components in the experimental setup, including cables, connectors, and even the copper traces on the circuit board, contributed non-negligible resistance to the fault circuit. In troubleshooting why the circuit breaker would not trip as expected, the resistance of the fault circuit measured approximately 100 mΩ, too resistive to cause a trip.

This issue of excessive resistance in the fault path necessitated a reconfiguration of the experimental setup. In an effort to reduce resistance various components were replaced or removed altogether. Initially, in an effort to preserve the scaled characteristic impedance of the cable between the circuit breaker and the fault insertion device, the BNC connectors at both end of the cables were removed and replaced with screw terminals. The BNC-terminated RG-58 cable was replaced with a three-foot length of bulk RG-8 cable without connectors. This did not reduce the fault resistance sufficiently because the cable's resistance was 20 mΩ. The entire experimental setup's fault resistance was only reduced by approximately 30 mΩ. Next, the scaled characteristic impedance of the cable connecting the circuit breaker and fault insertion device was sacrificed and the RG-8 cable removed. It was replaced with two pieces of 20 AWG magnet wire. Each 2-inch piece had a resistance of less than 1 mΩ. This substitution brought the resistance of the fault circuit, as measured from the output terminals of the circuit breaker, down to 32 mΩ. This modification to the experimental setup is acceptable because it simulates a fault at the circuit breaker's output terminals. Additionally, the measurement of interest would be affected by the

characteristic impedance of the input cable, not the output cable.

Ultimately, the reconfiguration efforts were insufficient to lower the fault circuit resistance far enough to allow the circuit breaker to detect the fault condition. The traces on the printed circuit board contribute enough resistance, perhaps 15 mΩ that achieving the maximum permissible fault resistance would not be possible using the current fault mechanism. The relay in the fault insertion device was replaced with transistor, but the initial spike in the fault current from the discharge of the load capacitance caused it to burn out. This meant that the next step involved redesigning the experimental setup by revisiting some of the calculations from Appendix C.

The redesign starts with redefining the fault conductance to a lower value that could be achieved in the construction of the experimental setup. This change breaks the scaling developed in Appendix C, but the change means that the circuit breaker is tripping on a less severe fault condition. As long as this lower $\frac{di}{dt}$ threshold is not exceeded by starting equipment on the circuit this is an acceptable change in the circuit breaker's characteristics. Setting the circuit breaker's sensitivity such that it can detect a short circuit caused by a 100 mΩ ground should allow adequate margin for the resistances in the circuit that cannot be eliminated by redesign. The model-scale fault conductance becomes

$$G_{fault,\ m} = \frac{1}{100\ m\Omega} = 10.0\ S$$

This requires a minimum capacitance of

$$C_{min,\ m} = \frac{2(215\ \mu F)(0.985\ A)}{(60.0\ V)(50.0\ S) - (0.985\ A)} = 1.20\ \mu F$$

This capacitance can be reasonably achieved with standard capacitor values. The minimum inductance required is

$$L_{min,\ m} = \left(\frac{1}{3}\right)(60.9\ \Omega)^2(1.20\ \mu F) = 1.48\ mH$$

Based on the cores used, this inductance requires 67.3 turns. Rounding up to 68 turns

will yield and inductance of 1.51 mH. This additional inductance will not negatively impact the circuit's protective function and will accommodate variation in the values of the capacitors when the circuit is assembled.

Again, the modification efforts did not result in a properly functioning circuit breaker. Another review of the relevant literature prompted a closer look at the thyristor. Though no references gave an explicit equation to calculate the turn-off time for the circuit breaker, Corzine[39] does mention using a thyristor with a turn-off time of 35 µsec. This is an order of magnitude faster than thyristor specified for previously for this study. To rule out slow thyristor turn-off as the source of improper circuit breaker functionality the Vishay VS-30TPS16 was replaced with an NTE Electronics NTE5463, whose maximum turn-off time is 25 µsec. The properties of this thyristor are summarized in Table D.3. This modification yielded a functioning circuit breaker and is what was ultimately used for testing in Chapter 4. The final circuit component selections are summarized in Table D.4 and the assembled redesigned circuit is shown in Figure D-8.

Table D.3. NTE5463 key characteristics.

Parameter	**Value**
Peak off-state voltage ($V_{peak,\ off}$)	200 V
Maximum RMS on-sate current (I_{RMS})	10 A
Maximum holding current, (I_L)	20 mA
Typical turn-off time, (t_q)	25 µs

Table D.4. Listing of main board circuit components for the final modified design.

Component	**Value**	**Part Number**
U1 (Thyristor)	N/A	NTE Electronics NTE5463
L1/L2	1.51 mH (68 turns)	EPCOS AG B66364B1016T001 EPCOS AG B66363G0000X127 EPCOS AG B66364A2000X000
C1-A/C2-A	1.20 µF	Parallel combination of 2×0.47 µF 0.27 µF 0.022 µF lab stock film capacitors
R1/R2 (Damping resistor)	1 Ω/5 W	N/A
R3 (Current limiting resistor)	1000 Ω	N/A
D1/D2 (Flyback diode)	N/A	IXYS DSI30-16A
D3 (Blocking diode, optional)	N/A	Omitted
SW1/SW2	Off-Mom	NKK Switches HP0215AFKP2-S
X1	N/A	Molex 0731375003
X2	N/A	Omitted
X3/X4	N/A	JST B3B-XH-A
X5/X6 (Optional)	N/A	JST B2B-XH-A

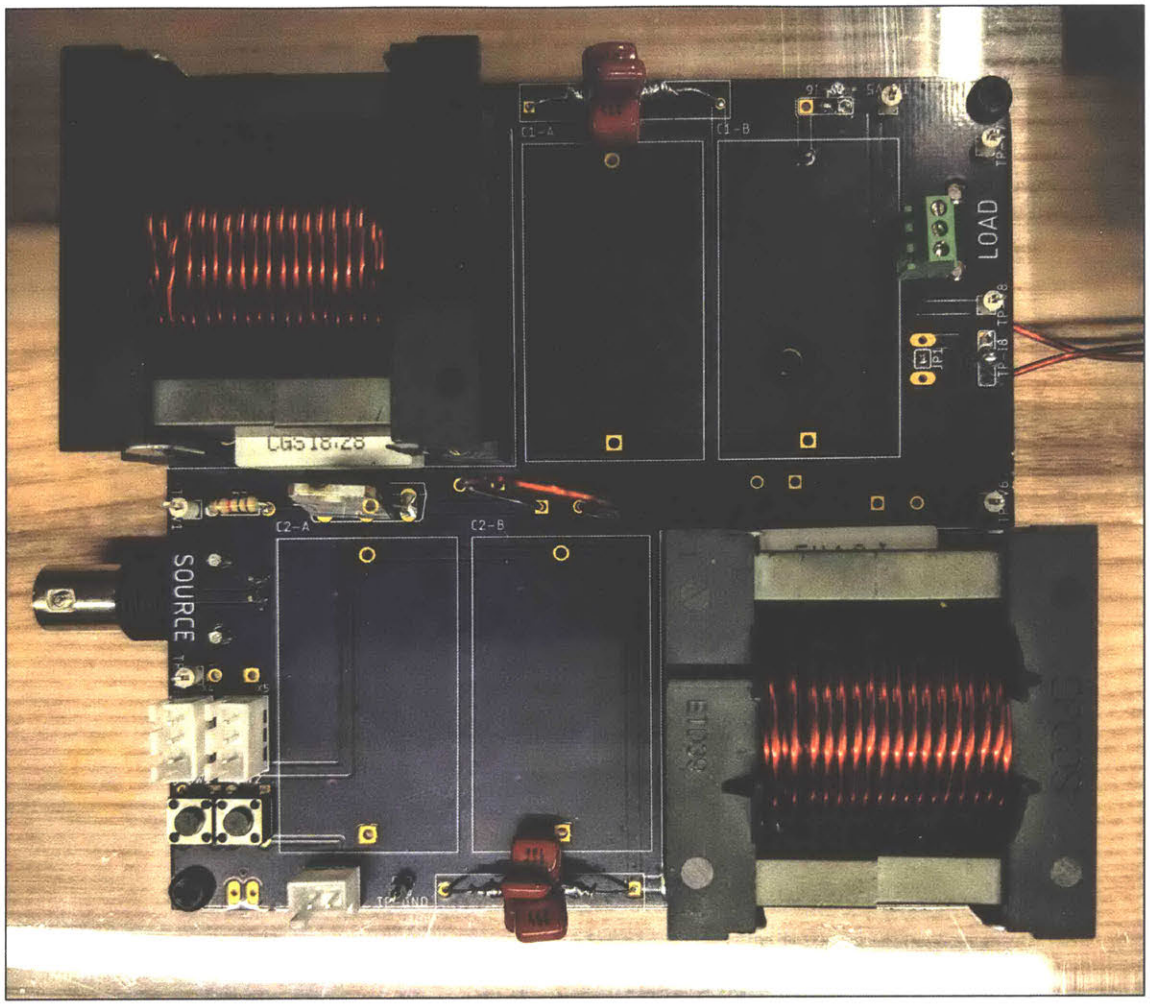

Figure D-8. The revised assembled model-scale z-source circuit breaker with components rated for 200 VDC.

THIS PAGE INTENTIONALLY LEFT BLANK

Bibliography

[1] E. Skjong, E. Rodskar, M. Molinas, T. A. Johansen, and J. Cunningham, "The marine vessel's electrical power system: From its birth to present day," *Proceedings of the IEEE*, vol. 103, no. 12, pp. 2410–2424, dec 2015. [Online]. Available: http://ieeexplore.ieee.org/document/7329674/

[2] Naval History and Heritage Command, "Electricity and USS Trenton," 2015. [Online]. Available: https://www.history.navy.mil/browse-by-topic/exploration-and-innovation/electricity-and-uss-trenton.html

[3] R. Burcher and L. Rydill, *Concepts In Submarine Design.*, ser. Cambridge ocean technology series: 2. Cambridge [England] ; New York : Cambridge University Press, 1994., 1994.

[4] Naval History and Heritage Command, "Langley I (CV-1)," 2016. [Online]. Available: https://www.history.navy.mil/research/histories/ship-histories/danfs/l/langley-i.html

[5] J. F. Hansen and F. Wendt, "History and state of the art in commercial electric ship propulsion, integrated power systems, and future trends," *Proceedings of the IEEE*, vol. PP, no. 99, pp. 1–14, 2015.

[6] J. S. Webster, H. Fireman, D. A. Allen, A. J. Mackenna, and J. C. Hootman, "Alternative Propulsion Methods for Surface Combatants and Amphibious Warfare Ships Chief of Naval Operations Combined Diesel or Gas Turbine," 2008.

[7] U.S. Navy, "The US Navy - Fact File: Destroyers - DDG," 2018. [Online]. Available: https://www.navy.mil/navydata/fact_display.asp?cid=4200&tid=900&ct=4

[8] U.S. Navy, "The US Navy - Fact File: Dry Cargo/Ammunition Ships - T-AKE," 2017. [Online]. Available: https://www.navy.mil/navydata/fact_display.asp?cid=4400&tid=500&ct=4

[9] T. J. McCoy, "Integrated power systems - An outline of requirements and functionalities for ships," *Proceedings of the IEEE*, vol. 103, no. 12, pp. 2276–2284, 2015.

[10] Naval Sea Systems Command, "Next Generation Integrated Power System: NGIPS Technology Development Roadmap," Naval Sea Systems Command, Washington, DC, Tech. Rep., 2007. [Online]. Available: http://www.dtic.mil/dtic/tr/fulltext/u2/a519753.pdf

[11] Naval Sea Systems Command, *Naval Ships' Technical Manual Chapter 300 Electric Plant - General.*

[12] H. G. Rickover and P. N. Ross, "Fault protection on shipboard A-C power-distribution systems," *Electrical Engineering*, vol. 63, no. 12, pp. 1099 – 1120, 1944.

[13] K. A. Corzine and R. W. Ashton, "A new z-source dc circuit breaker," in *2010 IEEE International Symposium on Industrial Electronics*, vol. 27, no. 6. Bari, Italy: IEEE, jul 2010, pp. 585–590.

[14] Naval Sea Systems Command, *Naval Ships' Technical Manual Chapter 320 Electrical Distribution Systems*, 6th ed. Washington, DC: Naval Sea Systems Command, 2010.

[15] Eaton, *Instructions for Installation , Operation and Maintenance of Type VCP-W Vacuum Circuit Breakers*, 03rd ed., Arden, NC, 2013.

[16] Naval Sea Systems Command, *Technical Manual for Main Switchboards, Port and Starboard, High Voltage (6.6KV).* Washington, DC: Naval Sea Systems Command, 1999.

[17] "IEEE Recommended Practice for 1 kV to 35 kV Medium-Voltage DC Power Systems on Ships," pp. 1–54, 2018.

[18] G. Chauncey, "Impedance measurement techniques in noisy medium voltage power hardware-in-the-loop environments," Ph.D. dissertation, Florida State University, 2018.

[19] F. Peng, "Z-source inverter," *Conference Record of the 2002 IEEE Industry Applications Conference. 37th IAS Annual Meeting (Cat. No.02CH37344)*, vol. 2, no. 2, pp. 775–781, 2003.

[20] K. A. Corzine and R. W. Ashton, "Structure and analysis of the z-source MVDC breaker," *2011 IEEE Electric Ship Technologies Symposium, ESTS 2011*, pp. 334–338, 2011.

[21] A. H. Chang, A. Avestruz, S. B. Leeb, and J. L. Kirtley, "Design of DC system protection," in *2013 IEEE Electric Ship Technologies Symposium (ESTS).* IEEE, apr 2013, pp. 500–508. [Online]. Available: http://ieeexplore.ieee.org/document/6523783/

[22] K. A. Corzine and R. W. Ashton, "A new z-source DC circuit breaker," *IEEE Transactions on Power Electronics*, vol. 27, no. 6, pp. 2796–2804, 2012.

[23] M. W. Aslam and N. A. Zaffar, "A novel bidirectional z-source DC circuit breaker for DC microgrids," *2016 IEEE 7th Power India International Conference, PIICON 2016*, 2017.

[24] D. Keshavarzi, T. Ghanbari, and E. Farjah, "A z-source-based bidirectional DC circuit breaker with fault current limitation and interruption capabilities," *IEEE Transactions on Power Electronics*, vol. 32, no. 9, pp. 6813–6822, 2017.

[25] D. J. Ryan, H. D. Torresan, and B. Bahrani, "A bidirectional series z-source circuit breaker," *IEEE Transactions on Power Electronics*, vol. 33, no. 9, pp. 7609–7621, 2018.

[26] J. G. Kassakian, M. F. Schlecht, and G. C. Verghese, *Principles of Power Electronics.*, ser. Addison-Wesley series in electrical engineering. Reading, Mass. : Addison-Wesley, c1991., 1991.

[27] J. L. Kirtley, *Electric Power Principles: Sources, Conversion, Distribution, and Use.* Chichester, West Sussex, U.K. ; Hoboken, N.J. : Wiley, 2010., 2010.

[28] H. Ravindra and J. S. Chalfant, "Email message to authors," November 29, 2018.

[29] C. Moton, "DDG 51 Flight III Update, presented to American Society of Naval Engineers," January 19, 2017.

[30] N. Doerry and J. Amy, "DC voltage interface standards for naval applications," *2015 IEEE Electric Ship Technologies Symposium, ESTS 2015*, pp. 318–325, 2015.

[31] M. Heidemann, G. Nikolic, A. Schnettler, A. Qawasmi, N. Soltau, and R. W. De Donker, "Circuit-breakers for medium-voltage DC grids," *2016 IEEE PES Transmission & Distribution Conference and Exposition-Latin America (PES T&D-LA)*, no. Mmc, pp. 1–6, 2016. [Online]. Available: http://ieeexplore.ieee.org/document/7914153/

[32] General Electric Company, J. C. Hey, and D. R. Grafham, *SCR Manual*, 5th ed. Semiconductor Products Dept., General Electric, 1972.

[33] X. Pei, O. Cwikowski, D. S. Vilchis-Rodriguez, M. Barnes, A. C. Smith, and R. Shuttleworth, "A review of technologies for MVDC circuit breakers," *IECON Proceedings (Industrial Electronics Conference)*, vol. 0, pp. 3799–3805, 2016.

[34] M. Kempkes, I. Roth, and M. Gaudreau, "Solid-state circuit breakers for medium voltage DC power," *2011 IEEE Electric Ship Technologies Symposium*, pp. 254–257, 2011. [Online]. Available: http://ieeexplore.ieee.org/document/5770877/

[35] J. Y. Kwen Chong, D. J. Ryan, H. D. Torresan, and B. Bahrani, "A buck converter with integrated circuit breaker," *IEEE International Symposium on Industrial Electronics*, vol. 2018-June, pp. 299–304, 2018.

[36] N. Doerry and J. V. Amy Jr., "Design considerations for a reference MVDC power system," *Transactions of the Society of Naval Architects & Marine Engineers*, vol. 124, pp. 40–59, jan 2016.

[37] Naval Sea Systems Command, "Naval Power Systems Technology Development Roadmap," Naval Sea Systems Command, Washington, DC, Tech. Rep., 2015.

[38] D. MacIsaac, G. Kanner, and G. Anderson, "Basic physics of the incandescent lamp (lightbulb)," *The Physics Teacher*, vol. 37, no. 9, pp. 520–525, dec 1999.

[39] K. Corzine, "DC micro grid protection with the z-source breaker," *IECON Proceedings (Industrial Electronics Conference)*, pp. 2197–2204, 2013.